A Critical Review of High Burnup Fuel Fragmentation, Relocation, and Dispersal under Loss-Of-Coolant Accident Conditions

Nathan Capps¹, Colby Jensen², Fabiola Cappia², Jason Harp¹, Kurt Terrani¹, Nicolas Woolstenhulme², Daniel Wachs²

¹Oak Ridge National Laboratory, Oak Ridge, TN 37831 ²Idaho National Laboratory, Idaho Falls, ID 83401

Abstract

High burnup fuel in excess of ~62–68 GWd/MTU has been observed to severely fragment when subjected to temperature transient conditions as in a loss-of-coolant accident. In the event of cladding failure, the severely fragmented fuel can relocate into the balloon region and potentially disperse through the burst opening into the reactor's primary system. This observation has led to implementation of several independent test programs designed to focus on various aspects of fuel fragmentation, relocation, and dispersal. The purpose of this review is to perform a critical, holistic assessment of fuel fragmentation, relocation, and dispersal under loss-of-coolant conditions to identify data gaps in the experimental data base. Phenomena have been identified and well defined through the various testing programs, and general agreement regarding the governing parameters (temperature, burnup, heating rate, cladding deformation, etc.) has been established. However, there is a significant data gap connecting research to commercial application. Furthermore, previous research has failed to evaluate the problem holistically. Major identified data gaps consist of (1) a comprehensive understanding of pretransient fuel rod conditions (fuel temperature, fuel stress, rod internal pressures, microstructure, etc.), (2) definition of prototypic loss-ofcoolant accident conditions (heating rate, fuel temperatures, fuel stress), (3) identification of the differences between nuclear and electrical integral loss-of-coolant accident tests, and connection of fuel rod performance (cladding ballooning, burst opening, potential relocation, fragmentation susceptibility, etc.) to fuel fragmentation, relocation, and dispersal severity. The content of this manuscript provides a clear path for connecting testing and data acquisition to commercial application by providing concrete means for filling data gaps and prioritized testing regimes.

1.0 Introduction/Background

The US nuclear industry is renewing efforts to build a technical basis to extend peak rod average burnup limits above the current regulatory burnup limit of 62 GWd/tU. The primary driver for these efforts is to economically increase cycle lengths of pressurized water reactors (PWRs) to 24 months, reduce the number of fresh fuel assemblies, and possibly reduce core design constraints. In order for US nuclear utilities to leverage these economic efficiencies, the US Nuclear Regulatory Commission (NRC) will likely require nuclear power plants (NPPs) to analyze a number of potential operational occurrences and their potential consequences with each new core design prior to resuming normal operation [1]. Utilities' current operating strategies are implemented to successfully verify that their NPP meets all safety criteria prescribed in 10 CFR 50.46 and 10 CFR 50.67 for an expected peak rod average burnup of 62 GWd/tU. However, US utilities are looking to extend fuel cycle operation to 24 months by increasing the peak rod average burnup beyond 62 GWd/tU. For PWRs to be able to extend fuel cycle lengths to 24 months, the peak rod average burnup is expected to reach 75 GWd/tU, with a peak pellet burnup of ~12% higher than the rod average [2]. For burnup extension, utilities must meet all current safety criteria by leveraging current licensing practices. Licensing concerns related to a loss-of-coolant accident (LOCA) including high burnup fuel have been discussed since the early 2000s.

The NRC generated Phenomena Identification Ranking Tables (PIRT) on high burnup fuel under LOCA to assess the performance of claddings during the high-temperature and quench phases of the transient [3].

¹ This manuscript has been authored by UT-Battelle, LLC under Contract No. DE-AC05-00OR22725 with the US Department of Energy (DOE). The US government retains and the publisher, by accepting the article for publication, acknowledges that the US government retains a nonexclusive, paid-up, irrevocable, worldwide license to publish or reproduce the published form of this manuscript, or allow others to do so, for US Government purposes. DOE will provide public access to these results of federally sponsored research in accordance with the DOE Public Access Plan (http://energy.gov/downloads/doe-public-access-plan).

¹ Corresponding author: cappsna@ornl.gov

The claddings' resilience under LOCA would likely be reduced since they would be increasingly degraded by extending service to high burnup. The design basis limits for these materials were historically determined by mechanical testing of irradiated cladding alloys under normal service conditions and subsequent semi-integral LOCA testing to determine their embrittlement thresholds. In general, the U.S. NRC expects the peak cladding temperature to remain below ~1,200°C and for the effective cladding reacted with steam to remain below 17% of its original cladding [3]. These specific design thresholds could potentially be modified for advanced claddings, but the general failure modes are not expected to change as burnup increases. High burnup data is required to confirm the general failure modes assumption. Consequently, new design limits for specific standard or advanced cladding designs under high burnup conditions could be proposed through similar mechanical testing and semi-integral test methods. Results from a recent PIRT study commissioned by the NRC on coated claddings [4] indicate that this model will also be expected for accident-tolerant fuel (ATF) technology. However, it implied that overall validation of cladding and fuel performance through integral tests will still be expected.

Following completion of the NRC PIRT studies, integral tests using the Halden reactor (and later in semi-integral tests at Studsvik) revealed that the response of high burnup fuel pellets under LOCA conditions could dramatically change from that historically observed [5]. Up to ~67 GWD/MT, fuel pellets were observed to fragment into pieces that were relatively large compared to the size of the cladding rupture, and relocation within the balloon region was modest. This phenomenon, termed *fuel crumbling during LOCA*, was well know and consequently deemed a low priority for investigation by the NRC [6,7,8]. However, the Halden and Studsvik tests that were conducted on fuel samples irradiated to >67 GWD/TU showed that fuel pellets could disintegrate or pulverize into extremely small particles. A significant fraction of these particles was fine enough to axially relocate within the balloon region or to be ejected out of the cladding rupture opening and into the reactor primary vessel (RPV). This phenomenon has since been termed *fuel fragmentation*, *relocation*, *and dispersal* (FFRD), and fuel pulverization termed *high burnup fuel fragmentation* (HBFF). FFRD could potentially invalidate some of the assumptions historically made to disposition licensing concerns related to core coolability as described in 10 CFR 50.46 [9], as well as assumptions related to source term [10].

As the industry moves toward higher burnups and increased enrichment, additional information is required to support the dispositioning of FFRD as a licensing concern. A number of assessments, reviews, and PIRT studies have been performed to highlight FFRD [3,11,12], and more specifically, HBFF. However, critical data reviews have provided little clarity regarding the research and development needed to adequately address the problem. A critical review of previous integral (i.e., Halden), semi-integral (i.e., NRC-sponsored), and separate effects tests is needed to form the foundation for further investigation. This manuscript presents a critical review of fuel fragmentation specific to fuel >62 GWd/tU under LOCA or temperature transients.

2.0 Current Understanding of LOCA

2.1 Pre-Transient Operating Conditions for High Burnup Fuel

Developing a test plan to investigate high burnup FFRD requires an understanding of the anticipated pretransient and transient operating conditions experienced by the fuel rod. High burnup core designs have yet to be deployed in the United States, resulting in a lack of operational data. However, tools used to evaluate core operating conditions have been used extensively to design and evaluate 18-month core designs to a peak rod average burnup of 62 GWd/tU. Based on this experience and drawing on advanced US Department of Energy (DOE) tools general understanding of pretransient and transient high burnup LOCA conditions can be gained. Zhang et al. [20] and Capps et al. [22] used DOE tools to investigate high burnup core designs and to assess fuel rod performance under steady-state and LOCA conditions.

Zhang et al. [20] developed a generic PWR model based on the South Texas Nuclear Power Generating Stations (STP Nuclear), a 4-loop Westinghouse PWR with a thermal rating of 3,853 MW_{th}. The model was developed to investigate fuel rod burst under LOCA for 24-month core designs using high

enrichment (6%) with increased burnup (peak rod average of 75 GWd/tU). Five core designs were evaluated to determine which would likely be considered for operation. However, only three core designs were evaluated throughout the LOCA transient. Fig. *I* and Fig. *2* illustrate the results for the fifth core design; the other analyzed core designs are presented in the evaluation performed by Hongbin et al. [20]. Fig. 1 indicates that 65 fuel assemblies contain high burnup fuel, at a rod average >62 GWd/tU. Of the 65 fuel assemblies, 32 are located on the periphery of the core, and the others are located in the center of the core. The peak rod average for the fuel rods in the center of the core range from >62 to 67 GWd/tU, and local burnups (i.e., peak pellet) range from and 66 to 72 GWd/tU. The peak rod average burnups on the periphery of the core range from a 69 to 76 GWd/tU, while the peak local burnup ranges from 74 to 81 GWd/tU. Fig. *2* provides the operating conditions for the hot rods (likely the most limiting during a LOCA) at the middle of cycle (MOC) and end of cycle (EOC). The results indicate that MOC onceburned fuel rods remain below 62 GWd/tU and would likely fall under the current LOCA safety criteria, whereas the hot fuel rods on the core periphery exceed 62 GWd/tU. Fuel rod operating conditions on the core's periphery range from 3–4 kW/ft., or ~10–13 kW/m. At EOC, once-burned fuel rods exceed 62 GWd/tU with a rod average linear heat rate (LHR) of 5–6 kW/ft., or ~16-20 kW/m.

DRAFT

Fig. 1. Burnup distribution at EOC for Core Design Option 5 [20].

Fig. 2. Average operating conditions for the hot rods at (a) MOC and (b) EOC for Core Design Option 5 [20].

Capps et al. [22] reported on the use of VERA to develop an equilibrium 24-month core design containing high burnup fuel with increased enrichment for a 4-loop Westinghouse PWR. The VERA results indicated that 96 fuel assemblies contained high burnup fuel rods (i.e., rod average >62 GWd/tU). The locations and rod average burnups of these fuel rods are shown in Fig. 3. The center of the core contained 13,736 high burnup fuel rods, whereas 1,050 were located on the core's periphery. The location of the high burnup fuel rods is consistent with the results reported by Zhang et al. [20], one exception being that the peak rod average burnup shown in Fig. 3 appears to be higher than the peak rod average burnups shown in Fig. 1. The rod average burnup distribution distribution for every high burnup (>62 GWd/tU) fuel rod in the center of the core is shown in Fig. 4. Fig. 5 provides the rod average peaking factor for every high burnup fuel rod in the core at EOC with a core average peaking factor of one, indicating an average LHR of 18.8 kW/m. The results indicate that high burnup fuel rods in the center of the core operate near the end of life with an average peaking factor ranging from ~0.9–1.1, which is equivalent to an average LHR of ~17 to 21 kW/m. High burnup fuel rods on the periphery of the core operate at lower average LHRs, <12 kW/m. Again, these results echo the results generated by Zhang et al. [20] and begin to show a clear pretransient operating regime for 4-loop Westinghouse PWRs operating for 24-month cycles. High burnup fuel rods fall into one of two operating regimes, and both regimes are consistent with the location of the fuel rods in the core (i.e., center and periphery of the core). For a 4-loop Westinghouse PWR operating for 24 months, fuel rods located in the center of the core have an EOC rod average ranging from 62-73 GWd/tU and a peak pellet burnup ranging from 68-77 GWd/tU. The rod average and peak LHR range from 16–21 kW/m and 18–24 kW/m, respectively. Fuel rods on the periphery of the core tend to have a wide range of burnups: the peak rod average burnup ranges between ~75–77 GWd/tU, and the peak pellet burnup ranges between 82-84 GWd/tU. However, these fuel rods experience rod average LHRs of ~10 kW/m and peak LHRs of <13 kW/m. Fig. 8 provides reference radial temperature profiles for fuel rods operating in the LHR regimes of interest. It should be noted that these temperature profiles may be subject to change, as the operating conditions and performance of the fuel can differ among various fuel suppliers and plants.

> Rod Average Burnup (GWd/tU)

Fig. 3. Location of every fuel rod with an average burnup greater than 62 GWd/tU at EOC [22].

Fig. 4. EOC rod average burnup distribution for every high burnup (>62 GWd/tU) rod in the center of the core [22].

DRAFT

Fig. 5. EOC rod average peaking for every high burnup (>62 GWd/tU) fuel rod in the core (core average LHR = 18.8 kW/m) [22].

Fig. 6. EOC temperature profiles calculated in high burnup fuel rods in the center of the core (23.7, 21.5, and 19.3 kW/m) and on the periphery of the core (less than or equal to 12.4 kW/m).

Fuel cracking is observed in both normal and accident conditions. The formation of radial, circumferential, and transverse cracks in UO₂ has been observed and understood under reactor startup, power changes, and shut down conditions [23–28]. Furthermore, UO₂ cracking has been evaluated using various analysis techniques (i.e., finite element, extended finite element, and phase field analyses) to assess the impact of UO₂ cracking on the overall performance of the fuel [24–31,Error! Reference source not found.]. In summary, this work indicates the pellet thermal gradiant, thermal expansion, and creep play an important role in crack nucleation and propagation. Fuel cracking and pulverization during a LOCA has been observed, however, the mechanism driving the phenomenon is still up for debate. Therefore, evaluating the changes in the fuel pellet stress state during a LOCA may provide a deeper understanding to the mechanisms that contribute to pellet pulverization. Fig. 7 evaluates the pretransient hoop, radial, and axial stress for a high-power (~21 kW/m) fuel rod.

The center of the pellet is in compression due to constrained thermal expansion with higher temperatures in the center and lower temperatures at the pellet surface. Moving radially toward the pellet periphery, hoop and axial stresses gradually become less compressive and effectively neutral. The expectation would be for tensile stresses to form on the pellet periphery resulting in cracking of the pellet to reduce stresses, however, cracking is currently not considered. Creep is governing the stress state across the pellet. At the pellet periphery, hoop and axial stresses become more compressive. This stress transition is a result of pellet-cladding contact. Higher temperatures result in higher axial and hoop tensile stresses on the cladding, and inversely, the cladding imposes compressive stresses on the pellet periphery. Radial stress is driven by thermal expansion with no external force acting in the radial direction, and therefore, fuel in the radial direction will be in compression throughout the pellet with the pellet outer surface being effectively stress free.

Fig. 7. Pre-transient hoop, radial, and axial stress profile in the fuel at the peak power location (~3.13 m from the bottom of the active fuel [22].

2.2 Transient Conditions for High Burnup Fuel

An example of a PWR fuel rod response during a double-ended guillotine break is illustrated in Fig. 8 [13]. The figure indicates three regimes that occur over the course of a LOCA: blowdown, refill, and reflood. Blowdown begins once rupture of the cold legs occurs and continues until the primary system depressurizes sufficiently. After the cold legs rupture, boiling occurs, and the coolant flashes to steam as causing the flow to reverse in a downward trajectory (downflow); the LOCA shuts down the fission process. High-power fuel rods rapidly exceed the critical heat flux (CHF) as downflow occurs. Exceeding the CHF results in a rapid decline in heat transfer between the fuel rod and the coolant, which rapidly increases the cladding temperature. Over the next few seconds, the remaining coolant in the primary system (core and loops) flashes to steam, reverses flow, and vacates the primary system through the rupture region. The flow through the break is high, but it is limited by critical flow phenomena. This results in flow saturation and reduction. Flow reduction could lead to a short period of time during which coolant flow reverses returning to an upflow condition, and along with the continued supply of coolant from intact loops, the cladding temperatures may reduce as some fuel rods may re-wet during this process. However, the pump's effectiveness reduces while two-phased flow exists, ultimately resulting in downflow to occur. Lastly, the heat source dramatically decreases as it transitions from fission to decay heat, further allowing cooling to take place. Overall, this process can take ~20–30 seconds to complete.

Fig. 8. Generic description of Zircaloy-4 fuel rod response during a double-ended cold leg break LOCA [13].

The refill phase overlaps some with the blowdown phase. Shortly after the break, the primary system pressure decreases to the point at which accumulators inject water into the cold legs and through the downcomer. However, the high steam flow typically redirects water out of the vessel and through the ruptured cold leg. Once the primary system approaches the containment pressure, the emergency core cooling system (ECCS) can successfully pump water at a high enough rate to penetrate the downcomer and begin refilling the lower plenum. This process occurs rather quickly, and reflooding begins once the ECCS injection reaches the core and the ECCS is able to successfully pump water into the core. However, reflooding of the core is occurring in an oscillatory state. ECCS coolant interacting with hot fuel rods generates steam, creating a two-phase flow system. The steam-water combination passes through the upper plenum of the core, through the hot leg, the steam generators, and the cold leg pump; eventually, the steam-water combination is vented through the rupture point. Steam generators continue to vaporize the water, further increasing the flow path resistance, and as a result, cladding temperatures continue to slowly increase. Eventually, the cladding temperature in the upper regions of the core begin to reduce as the heat transfer conditions transition from steam to dispersed droplet flow, and shortly thereafter, the core re-wets completely.

LOCA analysis methods have been developed and demonstrated by fuel suppliers [15,16,17], regulators [18,19], and other independent organizations [14,20,21]. These methods typically evaluate a number of different system responses and pretransient fuel conditions in accordance with the requirements outlined in 10 Code of Federal Regulation (CFR) 50.46, Appendix K. One important criterion is to ensure that the cladding temperature remains below 1,200°C. Zhang et al. [20] report the best estimate results shown in Fig. 9, which illustrates PCT RELAP results for the hot rods in each assembly. The results indicate that fresh fuel assemblies—or fuel assemblies in their first cycle of irradiation—had the highest peak cladding temperature (PCT) at EOC conditions, with the highest reported PCT being 648°C. Fuel assemblies in their second cycle of irradiation had lower PCTs ranging from ~800–830 °C. Third-burned fuel had even lower PCTs ranging from 413–460 °C. Capps et al. [22] evaluated fewer rods than Zhang et al. [20], but the PCT results for high burnup fuel were similar. Furthermore, Capps et al. [22] used a best estimate analysis to assess the PCT for a fresh fuel rod with the highest LHR at EOC (PCT = ~776 °C), and the results are consistent with TRACE results reported for a generic 4-loop Westinghouse PWR (PCT = ~826 °C) [19].

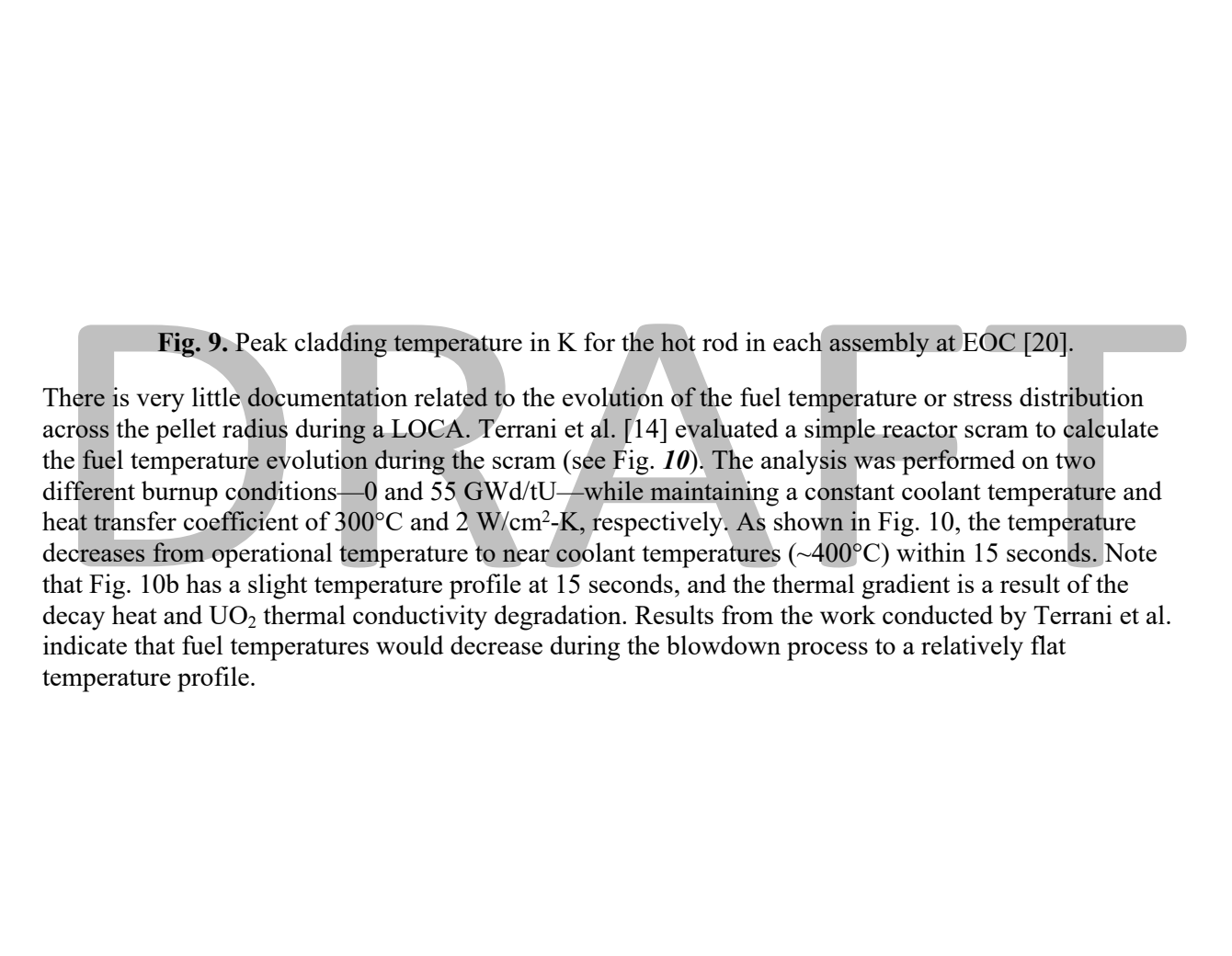


Fig. 10. Radial fuel temperature as a function of time following reactor scram with a constant coolant

temperature and coolant heat transfer coefficient of 300°C and 2 W/cm²K, respectively [14].

Capps et al. [22] performed a series of coupled RELAP5-3D transient thermal hydraulic and BISON 2-D R-Z fuel performance analyses to investigate fuel susceptibility to FFRD and conditions that lead to it. A secondary objective of this effort was to define prototypic LOCA conditions. The transient temperature evolution echoes the results generated by Terrani et al. [14]. Fuel temperatures are at steady-state operating conditions at the onset of a LOCA. However, the blowdown scrams the reactor and is able to sufficiently cool the fuel rod to coolant temperatures. As stated above, this process lasts $\sim 15-20$ seconds. At this point, the radial fuel temperature profile is effectively flat, and it slowly increases at a rate of ~8– 12°C/sec. This was calculated for high burnup (~71 GWd/tU) and lower burnup (~40 GWd/tU) fuel rods. Furthermore, the PCT and burst location were located near the pre-transient peak power. The BISON 2-D R-Z results shown Fig. 11 indicate that pretransient stresses are effectively neutral as a result of creep and cracking prior to the transient. Note that the equilibrium condition is formed with a steady-state temperature gradient. At the onset of the transient, the radial fuel temperature profile deviates from equilibrium to a flat profile and imposes tensile stresses in the center of the fuel and compressive stresses on the pellet periphery. Furthermore, these stress conditions persist as the mechanisms activating creep in UO₂ are inactive at low temperatures (<700°C) and in the absence of irradiation; see MATPRO UO₂ creep model for more details [149]. Furthermore, the timescale of the LOCA blowndown phase is order 15-30 seconds which is not enough time for UO₂ creep mechanisms to activate and reduce the stresses. Therefore, the expectation would be for tensile circumferential cracks, and possibly radial cracks, to form in the center of the fuel as a result of the rapid thermal contraction. The results indicate compressive circumferential and radial cracks may form on the pellet periphery. Cracks remove some of these constraints, which decreases stresses because the smaller fragments have a smaller variation in thermal expansion across their length. Therefore, this process indicates that the pretransient operating conditions impact the resultant equilibrium conditions (macro and micro) thereby affecting the stress state of the fuel pellet during the LOCA resulting in the formation of large fragments (i.e., >1 mm). However, these results shed little light on why fuel pulverization occurs during a LOCA.

Fig. 11. BISON 2-D R-Z results for radial (top left), hoop (top right), and axial (lower center) stress distribution across the fuel radius during a LOCA and at the burst location [22].

3.0 High Burnup LOCA Test and Data Analysis

3.1 Halden Reactor LOCA Test Rig Design and Execution

Decades of light-water reactor (LWR) fuel development programs across a handful of countries and their test reactors have seen various in-pile experimentation campaigns on LOCA behavior. These test methods differed in nuanced ways, but all shared the common aim of using internal nuclear heating and in-reactor environmental effects to investigate LOCA phenomena in the most prototypic way possible. A complete review of past in-reactor experimental LOCA programs can be found in works by Grandjean and the Organisation for Economic Co-operation and Development (OECD) [34,12,11]. The most recent of these test programs was hosted at the Halden Boiling Water Reactor (HBWR) in Norway; it began in 2003, entailed a total of 15 tests, and ended only recently with the closure of the HBWR plant. The HBWR test approach built on the rich legacy of preceding tests in other reactors. The HBWR LOCA test series (termed *IFA-650*) is probably most notable for being the first to address LWR fuels at burnup levels significantly beyond those addressed in previous programs.

A dedicated test rig was designed to support LOCA testing in the IFA-650 series. This rig was similar to many of the HBWR test rigs in which fuel specimens are placed in a tubular pressure flask with cooling water connections on the top. In the IFA-650 series, two water tubes, adjacent and parallel to the larger flask, routed inlet flow to and outlet flow from the bottom and top of the flask, respectively, for upflow water cooling during pre-LOCA irradiations. The entire rig was installed through the reactor top into the target test position of the HBWR core, where it was connected to out-of-reactor hydraulic support equipment (e.g., pumps, heat exchangers) to complete the coolant loop. The coolant loop provided forced convection pressurized liquid water cooling during pre-LOCA irradiations. These pre-LOCA irradiations were used for specimen power calibrations and for accumulating short-lived radioisotope inventories to suit test objectives. Deuterated water, which was also used to cool HBWR's primary core circuit, was also used to cool these LWR specimens. A cylindrical flow tube surrounded the test rod to achieve the desired heat transfer conditions. This flow tube also had embedded electrical resistance heaters to simulate hot neighboring rods in a fuel bundle during the LOCA segment of the test evolution. Thermocouples (TCs) were placed in the test rig to measure environmental conditions, including flask inlet/outlet temperature and heater wall temperature.

After the steady-state irradiation with liquid water cooling, the LOCA test sequence occurred by reducing reactor power to induce 10–30 W/cm linear heating rate in the rod, followed by manipulation of system valves to isolate a smaller coolant circuit from the remainder of the loop, including the pump, in a cooling mode driven by natural circulation. The blowdown valve was then opened, causing the pressurized water inventory to drain quickly to a large ex-reactor tank, and the continued fission heating in the test rod caused its temperature to steadily climb. Electrical current was provided to the flow tube heater shroud to heat up concurrently with the rod. In some tests, a small tube in the test rig was used to inject water spray near the test rod so that adequate steam was present for post-burst internal cladding oxidation. The tests were terminated 5 minutes after the blowdown when the reactor was shut down and the heater shroud was deenergized. The test rod then cooled slowly in the dry flask since it was determined that injection of liquid water could disrupt the state of the specimen and the valuable data objectives that posttest forensics would entail. Finally, the test rod was scanned by a special-purpose gamma spectroscopy apparatus to provide data about the fuel's geometric state prior to orienting the rig horizontally for shipment to shielded cells for posttest examinations.

The typical fuel rod specimen in the IFA-650 tests had a fueled length of 50 cm, and apart from the two commissioning irradiations performed on fresh fuel rods, they were cropped from longer rods that had been irradiated in commercial power plants, including PWR, boiling water reactor (BWR), and water-

water energetic reactor (VVER) types. Test segments were carefully selected to achieve specimens with the desired burnup profile and proximity to features such as grid spacers. These rods were refabricated with new welded end caps and re-pressurized with plenum gas to simulate the desired cladding stress state during LOCA testing. These new rod end caps and interfacing test rig hardware supported various sensors. Rod refabrication was performed in shielded hot cell facilities prior to irradiation in the HBWR. Internal pressure in the rod's upper plenum was measured by a small sealed metallic bellows which compressed as pressure increased, causing translation of a small ferritic core to be measured by a linear variable differential transformer (LVDT). Another small ferritic core was mechanically connected to the upper end cap so that cladding axial elongation could be measured by another LVDT. The pressure sensor crucially indicated the timing and pressure of rod internal pressure, including burst events. The elongation sensor identified timing of cladding balloon formation as manifested by discontinuous indications compared to the otherwise smooth trend arising from thermal expansion alone.

Small metal sheathed TCs measured cladding surface temperature. These TCs were held against the cladding surface by thin metallic straps welded to the cladding. Care was taken to place TCs above and below the peak temperature axial region where ballooning was expected to avoid creating anomalous performance at the TC site. Apart from fresh fuel commissioning tests, TCs were not placed into the fuel centerline itself during the subject irradiations. Hence, the thermomechanical state of high burnup fuel pellets arising from radial temperature gradients was largely inferred based on thermal models and cladding temperature measurements. Lastly, vanadium-emitter self-powered neutron detectors (SPNDs) became the mainstay neutron flux measurement device in the IFA-650 test series. Three of these SPNDs were distributed axially in the rig and helped measure the neutron flux delivered to the test rig while also giving some indication of fuel relocation in the test specimen. More detail on the IFA-650 test series can be found in works by Wiesenack [35 and 36].

DRAFT

Fig. 12. Schematic of Instrumented Fuel Assembly (IFA) 650 LOCA test rig with instrument levels [33]

3.2 LOCA Furnace Test Rig Design and Execution

High burnup LOCA tests performed at Argonne National Laboratory (ANL) were originally designed to evaluate the mechanical response of the cladding after a LOCA transient [34]. The focus of the tests was to understand the role of the cladding's outer surface oxide layer, as well as pre-transient hydrogen concentration on post-quench ductility. Subsequent LOCA test rig designs used the system that was initially designed an operated at ANL as the reference for subsequent electrical heating LOCA tests [34–39]. In general, the LOCA test stations are all very similar, with the greatest difference being that the Studsvik LOCA test station uses 3 N axial weight in an attempt to preserve the axially straight nature of the rodlet during the transient [38,44]. It remains unclear how the axial counterweight impacts the LOCA results. The weight does apply an additional and constant axial load to the cladding prior to and throughout the LOCA transient. It is unclear whether the apparatus allowing the weight to be hung from the bottom of the rod actually constrains axial expansion of the cladding as it heats up. If it indeed acts to

constrain the cladding axial expansion, then it is defeating its original purpose and may be exacerbating cladding ballooning.

Electrically heated LOCA test rig designs [34–39] use infrared (IR) radiation to heat fuel segments ranging from 200–300 mm in length, or the approximate distance between two spacer grids. The fuel rod segments are pressurized and placed in a quartz tube with flowing steam or argon. The quartz tube affords the opportunity to quench the rodlet after the LOCA heating phase.

Electrically heated high burnup LOCA tests typically pressurize each rodlet with helium to pressures ranging from 8-11 MPa. The rod internal pressure is intended to be representative of end-of-life conditions as typically observed in commercial LWR fuel. Each LOCA test follows a similar temperature transient. The transient begins with an initial heat-up to ~300°C to test the ability of the rodlet to hold pressure and to ensure that TCs are working correctly. Once the initial heat-up is complete, rodlets are heated at a rate of 5°C/sec until the terminal temperature (often 1,200°C) is reached. The rodlets are then cooled to 700-1,000°C at a constant rate, followed by water quenching. Fig. 13 provides an example of a typical LOCA transient sequence for electrically heated rodlets. The sequence is controlled by a computer and monitored by several TCs which are attached in a couple of different ways. The manner in which the TCs are attached may impact the response of the rodlet during the LOCA. In a LOCA test performed at ANL four Type S TCs were spot-welded to each rodlet [34], two of which were spot-welded at the midplane in the expected burst location 180° apart, and the other two were spot-welded approximately 50 mm above and below the rodlet midplane. Studsvik, however, used a clamp to attach a single N Type TC approximately 50 mm above the axial midplane. The clamped TC was attached with an Inconel X-750 clamp (Fig. 14a). As shown in Fig. 14b, the clamp is located approximately 25 mm above the burst focal point, so the potential exists for undue stress to be applied to the cladding, restricting the ability of the balloon to expand. OCL LOCA tests at ORNL used either spot-welded or wire-wrapped TCs in the same locations that were used in the ANL in-cell LOCA (ICL) test. The ORNL SATS tests used wire-wrapped TCs on the rodlet. Wire wrapping the TCs presents the same concern as the clamp if they are in the vicinity of the burst and ballooned region. At this point, any conclusions drawn from the techniques used to attach the TCs is merely conjecture. However, a review of the experimental and post-irradiation examination (PIE) data may illuminate whether the techniques used to attach the TCs are problematic or not.

Fig. 13. Schematic describing the time-dependent temperature conditions for ICL transients [34].

(a) (b)

Fig. 14. a)Image of the Inconel X-750 clamp [38], used to attach the thermocouple to the rodlet for the Studsvik ICL, and b) schematic [38] illustrating the expected balloon size and burst location in relation to the thermocouple location.

Table 1 provide a summary of the electrically heated LOCA tests. The out-of-cell and in-cell test conditions are relatively similar in nature across the programs, with a couple of significant differences. OCL LOCA tests, specifically ANL's OCL series and ORNL's 21–23 series, used zirconia pellets as UO₂ surrogates. These tests focused on developing test data on unirradiated cladding samples in order to compare the results to irradiated samples. Additionally, ANL evaluated the impact of environmental conditions by comparing Zircaloy performance in steam and argon conditions. Rodlet material and geometries differed greatly across the programs. The ANL LOCA test used as-fabricated BWR Zry-2 cladding and harvested rodlets from fuel rods that had been irradiated in Limerick. The father rods accumulated a rod average burnup of ~56–57 GWd/tU [34]. The rodlet burnups were higher, as they were extracted from the peak burnup regions located in the upper portions of the fuel rods. Fuel rods used for the NRC-sponsored LOCA test were irradiated in an unspecified PWR to a burnup of 55.2 and 68-69 GWd/tU. Each rod was geometrically identical in the as-fabricated state, and the cladding material was identified as ZIRLO. Four rodlets were harvested from the high burnup fuel rods (i.e., 68-69 GWd/tU), and two rodlets were extracted from the lower burnup fuel rods (i.e., 55 GWd/tU). Rodlet burnups were not listed in the NUREG reports. However, rodlet burnups were reported by Sonnenburg et al. and Turnbull et al. [41,42]. The rodlets extracted from the high burnup fuel rods ranged from 72–78 GWd/tU, whereas the rodlets harvested from the low burnup fuel rods ranged from 60-61 GWd/tU. Lastly, the LOCA tests performed at ORNL were performed on two different types of PWR cladding materials and two different fuel rod geometries. Four tests were performed on Zry-4, and two tests were performed on M5. The rodlet geometries are identical with the exception of the rodlet irradiated in HB Robinson. Three out-of-cell tests were performed on as-fabricated Zry-4 cladding tubes, and three ICL tests were performed on irradiated rodlets. The irradiated rodlets were harvested from three different fuel rods, and the average burnups for the father rods are 66.5, 67, and 75 GWd/tU. Jadernas et al. [43] provides gamma scans for each fuel rod, as well as the axial location of each rodlet, making it possible to determine the burnup of each rodlet. The respective burnup for each rodlet is 71, 74, and 84 GWd/tU.

Table 1Summary of the OCL and ICL performed at ANL [34], NRC sponsored high burnup LOCA test performed at Studsvik [8,40], and Nuclear Science User Facilities (NSUF)-sponsored high burnup LOCA test performed at ORNL [39]

Fuel Rod ID	Irradiation Condition	Testing Environment	Materials	Father rod burnup (GWd/tU)	Rodlet burnup (GWd/tU)	Outside diameter (mm)	Wall thickness (mm)	pressure at 300°C (MPa)	Hold temperature (°C)	Hold time (s)
-------------	--------------------------	------------------------	-----------	----------------------------------	------------------------------	-----------------------------	---------------------------	-------------------------------	-----------------------------	------------------

Internal

OCL#5	Unirradiated	Argon	Zry-2	0	0	11.18	0.71	8.28	-	-
OCL#8	Unirradiated	Argon	Zry-2	0	0	11.18	0.71	8.28	-	-
OCL#11	Unirradiated	Steam	Zry-2	0	0	11.18	0.71	8.28	1024	300
OCL#13	Unirradiated	Steam	Zry-2	0	0	11.18	0.71	8.28	1024	300
OCL#22	Unirradiated	Steam	Zry-2	0	0	11.18	0.71	8.28	1024	300
ICL#1	Limerick	Argon	Zry-2	56	68	11.18	0.71	8.28	1024	300
ICL#2	Limerick	Steam	Zry-2	56	61	11.18	0.71	8.28	-	-
ICL#3	Limerick	Steam	Zry-2	56	66	11.18	0.71	8.28	1024	300
ICL#4	Limerick	Steam	Zry-2	56	67	11.18	0.71	8.28	1024	300
189	US PWR	Steam	ZIRLO	68.2	72	9.5	0.57	11.14	950	-
191	US PWR	Steam	ZIRLO	69.3	75	9.5	0.57	11.14	1185	25
192	US PWR	Steam	ZIRLO	68.2	78	9.5	0.57	8.3	1185	5
193	US PWR	Steam	ZIRLO	69.3	76	9.5	0.57	8.3	1185	85
196	US PWR	Steam	ZIRLO	55.2	61	9.5	0.57	8.3	950	-
198	US PWR	Steam	ZIRLO	55.2	60	9.5	0.57	8.3	1185	85
23	Unirradiated	Steam	Zry-4	0	0	9.5	0.57	4.14	1200	135
21	Unirradiated	Steam	Zry-4	0	0	9.5	0.57	6.21	1200	110
22	Unirradiated	Steam	Zry-4	0	0	9.5	0.57	8.27	1200	90
HBR#1	HB Robinson	Steam	Zry-4	66.5	41	10.77	0.76	8.27	1000	120
NA#1	North Anna	Steam	M5	67	74	9.5	0.57	8.27	1200	90
NA#2	North Anna	Steam	M5	75.1	84	9.5	0.57	8.27	1000	-

3.3 In-Situ Observations and Post LOCA PIE

3.3.1 Cladding Behavior under LOCA Heating Conditions

ICL and OCL tests performed temperature transients similar to the one shown in Fig. 13. From test to test, the major differences consisted of fuel irradiation conditions (i.e., BWR vs. PWR), rodlet burnup,

cladding type, fuel rod geometry, and pre-transient rod internal pressure, as shown in Table 1. Each rodlet was heated from 300°C to a terminal temperature at a rate of 5°C/sec. Burst timing was assessed by measuring the rod's internal pressure throughout the experiment. Fig. 15 provides the experimental measurements taken during the NRC-Studsvik LOCA experiments for each rodlet [40], and similar figures can be found in work by Grandjean, as well as Helin and Flygare [34,39]. The rodlets show distinct difference in pressure drop following burst. Rodlets 196 and 198 did not experience significant fragmentation, whereas the other rodlets did. Rodlets that experienced severe fragmentation and relocation appear to experience a slower depressurization rate compared to the other rodlets. The mechanism driving this is unclear, but one theory could be that the fragmentation process generated additional fission gas which contributed to increasing the pressure temporarily. However, fission gas release (FGR) was not measured during the experiment, so it is not possible to confirm this theory. Work funded by the NRC [44] evaluated transient axial gas transport on fuel rods with lower rod average burnups of ~35 GWd/tU. However, the LOCA de-pressurization results appear to echo the transient axial gas transport test performed in reference [44] and shown in Fig. 16. The experiments performed as described in the work by Dagbjartsson et al. [44] were designed to evaluate how changes in fuel rod geometry (i.e., pellet-cladding gap and fuel crack networks) affect gas transport throughout the fuel rod, and while the tests were performed on lower burnup fuel, the de-pressurization trend appears to hold at high burnups, as well.

DRAFT

Fig. 15. Summary of the NRC-sponsored LOCA test pressure history immediately following rupture [40].

Fig. 16. Transient flow test evaluating the impact of axial gas transport through a fuel rod as extracted from reference [44].

The first phenomenon occurring during a LOCA transient is bending. Bending is attributed to anisotropic creep and plastic deformation that occurs in alpha-phase zirconium at temperatures near the alpha-beta transition temperature with application of a constant internal pressure [37]. This phenomenon has been observed in all LOCA tests to date. LOCA tests at ANL observed bending through real-time videos and indicated that bending occurred prior to the ballooning process [37]. Furthermore, this phenomenon was observed in the ORNL OCL test, as shown in Fig. 17, and the results [39] confirm the theory suggesting that rod internal pressure drives anisotropic creep and plasticity in the cladding. As seen in Fig. 17, Zr-19 has a rod internal pressure of 0 MPa, and bending was not observed. As the rod internal pressure increases, hoop stress begins activating cladding creep, and bending becomes more pronounced, as seen in Zr-22. These tests, however, were performed on unirradiated cladding. Billone et al. compared unirradiated and irradiated LOCA test results and noted that the amount of bending in high burnup cladding was noticeably less than that of unirradiated cladding [37], possibly a result of irradiation hardening, oxidation, and hydrogen pickup. It was also noted that the proclivity of the burst opening occurred on the concave side of the rodlet. The NRC-sponsored LOCA test observed bending in rodlet 191, which had an initial rod internal pressure of 11.1 MPa at 300°C, as seen in Fig. 18. However, the experimental summary documented this as a distortion and modified the test train in order to prevent bending from occurring [38,40]. It was later verified that the modification prevented bending in subsequent test segments [38,40]. However, the impact of the test train modifications on fuel rod performance remains unclear, so it is simply suggested here that these changes likely altered the prototypic behavior.

Fig. 17. Rodlet bending under LOCA conditions as a function of rod internal pressure [39].

Fig. 18. Rodlet 191 bending under LOCA conditions during the NRC-sponsored LOCA test [40].

The cladding begins to balloon immediately following bending until burst occurs. This process was visibly observed and reported by Billion [37]. The extent of cladding ballooning is reliant on a number of parameters; however, heating rate is the primary parameter which ultimately dictates the time available for creep processes to occur. Experimental data [45,46,61] shows a clear relationship between hoop strain at the burst location and cladding heating rate. Slow heating rates provide more time for creep, resulting in larger balloon strains below 950°C, whereas smaller balloon strains are observed above 950°C. The opposite is true for fast heating rates. Powers et al. [45] developed two correlations to define the maximum hoop strain as defined by heating rate (Fig. 19). The first considers heating rates less than or equal to 10°C/sec, while the second considers heating rates greater than or equal to 25°C/sec. The correlations developed by Powers et al. include three temperature regimes, but high burnup cladding burst data suggest that burst occurs between 700 and 950°C, so, higher temperature strain peaks are not shown.



Fig. 19. LOCA Burst hoop strain data as a function of burst temperature compared Powers et al. cladding hoop strain relationship [11,45,46,48–60].

Electrically heated high burnup LOCA tests heated rodlets at a rate of 5°C/sec, while in-pile LOCA tests at Halden used heatup rates that started at ~4.2°C/sec and decreased to <1°C/sec. Halden reported diametral strain and not hoop strain, which is why Halden data are not reported in Fig. 19. Therefore, the most appropriate curve for comparison is less than or equal to 10°C/sec. Most of the data in Fig. 19 fall below the peak threshold. Zircaloy begins transitioning from alpha to beta phase at around 900°C, where alloying additions and dissolved oxygen and hydrogen in the cladding greatly affect the transition temperature [62]. Additional uncertainty is expected, as each cladding sample will behave based on the stage of transition. Rodlets that fail at lower temperatures, specifically the NRC-Studsvik rodlets, are more curious. Data presented by Powers et al. [45] suggest that cladding ballooning should be minimal until the cladding temperature exceeds ~700°C. It is not clear what caused these rodlets to have such a high hoop strain at such low temperatures, especially after being previously irradiated in a PWR. The axial weight intended to prevent bending may have provided additional stress, resulting in additional ballooning.

One concern is that all of these various LOCA tests were conducted under non-prototypic conditions or conditions that may not be appropriate for every reactor type. Analysis performed by Zhang [20] indicated that cladding heating rates observed in PWRs should evolve throughout the LOCA event. At the onset of the LOCA, cladding temperatures calculated by Zhang suggest that cladding heating rates in the first 10–20 seconds should be on the order of ~24–34°C/sec and then should decrease to ~2–5°C/sec. Similar observations were made by Terrani [14]. Work performed by Erbacher [47] and Raynaud [19] echo the heating rates calculated by Zhang et al. and further indicate that cladding heating rates depend on the pre-transient power of the rod and surrounding fuel rods. Heating rates for a 4-loop Westinghouse PWR as calculated by Capps [22] indicate that heating rates should range between ~8–12°C/sec. This implies that LOCA test results to date are non-prototypic for a generic 4-loop Westinghouse PWR. However, 5 °C/sec may be appropriate for different or more specific PWR designs; specific fuel assembly designs may impact LOCA heating rates as well." For example, some reported heating rates [19,47,20] suggest that the cladding hoop strain would be at least a factor of two less based on the peak hoop strain correlations presented in Fig. 19. Secondly, the cladding under these heating rates would likely burst at higher temperatures. The Chapman burst relationship suggests that cladding with a burst stress of 70 MPa would burst at 750°C for a heating rate of 5°C/sec and 830°C for a heating rate of 28°C/sec. Additional factors could result in reduced fuel fragmentation, as will be discussed below. It should be noted that heating rates may transition from 24–34°C/sec to 2–5°C/sec at a temperature lower than the burst temperature, and there is no clear indication how this transition might impact the response of the cladding. However, the current data do offer an unexpected benefit, as the data are overly conservative.

Cladding burst prevents further cladding deformation, as the driving force is vacated through the burst opening. Fig. 20 summarizes integral LOCA test burst data and compares that data to the burst relationship developed by Chapman [45,46]. In general, the burst relationship agrees fairly well with the data. However, there are a few outliers. With the Halden 650.X series, the heating rate started at ~4.2°C/sec and decreased to <1°C/sec. The burst relationship, as shown in Fig. 20, is specific to 5°C/sec; the Chapman model indicates that the burst stress decreases as heating rates decrease. Therefore, adjusting the Chapman model heating rate would result in better and possibly conservative agreement. Unirradiated rodlets are slightly below the Chapman burst model. A possible reason for this might be a lack of zirconium oxide and hydrogen on and in the cladding. Erbacher et al. assessed the impact of oxygen and hydrogen uptake on cladding embrittlement and burst [47] and determined that cladding oxidation had an impact, although it was small. Observations made by Billion [37] indicate differences between high burnup and unirradiated cladding behavior during the temperature transient, and they attribute these differences to cladding embrittlement mechanisms: specifically oxidation and hydrogen uptake [37]. This leads to the conclusion that high burnup cladding is expected to burst at higher stresses than unirradiated cladding, so the unirradiated cladding is expected to burst at lower stresses. There are, however, a few outliers—specifically the NRC-sponsored test—that do not have a simple explanation. When comparing the hoop stress from the NRC-sponsored test to the Chapman burst relationship, the Chapman relationship indicates that four rodlets were expected to burst at ~750°C with a hoop stress of 65–70 MPa, whereas the two remaining rodlets were expected to burst at ~700°C with a hoop stress of ~90 MPa. The two rodlets expected to fail at ~700°C and ~90 MPa are identified as rodlet 189 and 191. Burst results for these two tests agree fairly well with the Chapman relationship, considering the initial internal pressures for these rods were 11.1 MPa. The four remaining rodlets had an initial pressure of 8.3 MPa and are well below the Chapman relationship. Work by Flanagan et al. [40] indicates that rodlet 189 and 191 were tested under a different set of conditions than the other four rodlets. Severe bending was observed in rodlet 191 (Fig. 18) as a result of high-temperature anisotropic creep and cladding plasticity. This phenomenon was observed in previous LOCA tests [34,39,54–60], and results generated at ORNL [39] demonstrate that increasing rod internal pressure increases bending severity. However, there was speculation that a small axial constraint was being applied to rodlet 191 that caused bending to occur, and in order to prevent bending, subsequent LOCA tests would incorporate an axial weight to counterbalance the speculated axial constraint. Application of the counterweight causes serious concern, as the weight

was intended to prevent a naturally occurring phenomenon, and when comparing the result to other LOCA tests performed under similar conditions, the axial weight resulted in rodlets failing prematurely. Furthermore, the additional stress imposed by the axial weight may have resulted in larger balloon and burst sizes. Lastly, the ramifications of burst occurring at lower temperatures may exacerbate the fragmentation and relocation behavior of the fuel.

Fig. 20. Summary of the cladding burst results for all integral/semi integral LOCA test compared to the burst curve developed by Chapman et al. [11,45,46,48–62].

Fuel dispersal is reliant on the size of the burst opening. Burst opening data generated through various LOCA and cladding balloon-burst test programs show no indication that burst width or length is dependent on burnup (see Fig. 21a and b). Data generated at ANL and ORNL indicate that there is a difference in the burst shape as it pertains to unirradiated and irradiated cladding. Unirradiated cladding fractures in a ductile manner in which the width of the opening collapses inward (termed dog bone), whereas previously irradiated cladding fractures in a brittle fashion, with an open mouth burst shape (termed oval). A contributing factor may be the relationship between the width and length of the burst opening, as shown in Fig. 21c. The burst width is two fifths of the burst length until the burst length reaches 20 mm; the width of the burst saturates at ~10 mm, irrespective of burst length. This saturation directly correlates to the outer diameter of the cladding. The length of the burst correlates to the balloon deformation characteristics, as shown in Fig. 21d. The burst length increases as the hoop strain increases. These data, however, are representative of <10°C/sec heating rates, and as discussed above, heating rates in PWRs range from 24–34°C/sec, and then they decrease to ~2–5°C/sec. It is unclear how changing the heating rate will impact the burst size. However, it is clear that the size of the balloon directly impacts the burst opening and points to the significance of understanding the cladding behavioral evolution under prototypic temperature transient conditions. Future work must focus on generating fuel rod behavior data under prototypic PWR conditions so that more reliable conclusions can be developed.

a b

DRAFT

c d

Fig. 21. (a) Burst width and (b) burst length as a function of rodlet average burnup, (c) burst width as a function of burst length, and (d) burst length as a function of hoop strain for all integral/semi integral LOCA test [48–62].

3.3.2 High Burnup UO₂ Behavior under LOCA Heating Conditions

Up to this point, the focus of this work has been on the cladding response under LOCA conditions. This response is critical, as FFRD should be addressed holistically. Integral and semi-integral LOCA tests were originally designed to evaluate cladding performance (balloon and post-quench ductility), but following the Halden IFA 650.X test, LOCA tests were designed to specifically evaluate fuel fragmentation and potential dispersal under high burnup conditions. Yueh et al. [63] define high burnup fuel fragmentation (HBFF) by fragment size:

Large fragments: >2 mm
 Medium fragments 1-2 mm
 Fine fragments <1 mm

The volume of large fragments (i.e., >2 mm) is approximately half the size of a UO₂ fuel pellet, while medium size fragments (i.e., 1–2 mm) are approximately a quarter the size of a UO₂ fuel pellet. Fine fragments (i.e., <1 mm) range from powder to very small fragments. Images of the fuel fragment distribution from the NA#2 high burnup LOCA test are shown in Fig. 22.

Fig. 22. HBFF images [39] of NA#2 high burnup LOCA test performed at the Sever Accident Test Station: (a–d) fine fragments < 1 mm, (e) medium fragments ranging from 1–2 mm, and (f) large fragments >2 mm.

Table 2 summarizes high burnup LOCA tests as a function of rodlet burnup, terminal temperature, and fragmentation data, and Fig. 23 assesses the relationship between mass fraction of UO₂ fragments less than 1 mm to burnup and terminal temperature. There is a clear relationship between rodlet burnup and an increase in fine fragmentation. The trend suggests that fine fragmentation does not occur for rodlet burnups below 71 GWd/tU. However, above 71 GWd/tU, fine fragmentation increases to ~100% as the rodlet burnup exceeds ~82-83 GWd/tU. It should be noted that sieve data do not exist for Halden 650.3, 4, 5, and 9, and for these tests, Halden reported that the fuel fragmented into medium (i.e., 1–2 mm) and fine (i.e., <1 mm) fragments. Therefore, it was conservatively assumed that 100% of the pellet fragmented into <1 mm particles. Increasing terminal fuel temperatures also correlates to an increase in fine pellet fragmentation. The trend suggests that fine fragments do not form below 800°C. There is, however, a data gap at terminal temperatures <800°C, and given results reported by P. Raynaud et al. [19], it seems most appropriate for subsequent tests to focus on terminal temperatures ranging from 750– 850°C. However, the correlation has outliers, specifically rodlet average burnups >82 GWd/tU. Again, sieve data are not available for these specific Halden tests and may be an over estimation. Future LOCA tests should evaluate a variety of rodlet burnups ranging from 71-84 GWd/tU at terminal temperatures ranging from 750-850°C as this seems to be consistent with anticipated PWR operating regimes. Tests to date have developed a burnup fragmentation trend for terminal temperatures greater than or equal to 1,000°C. Of course, prototypic terminal temperatures must be verified to ensure the data spans the appropriate operating PWR conditions.

Table 2Summary of the fragmented fuel particles collected from LOCA fragmentation tests [39]

	Test series	Test number	Burnup (GWd/tU)	Terminal temperature (C)	Mass fraction < 1 mm (%)	Mass fraction < 0.5 mm (%)
-			` ′	(C)	` ′	` ′

	189	72 (68.2)+	950	No data	No data
	191	75 (69.3)+	1185	67.67	46.34
Studsvik	192	78 (68.2)+	1185	69.31	55.26
Studsvik	193	76 (69.2)+	1185	58.62	41.75
	196	61 (55.2)+	950	0.00	0.00
	198	60 (55.2)+	1185	0.00	0.00
	650.12	72.3	800	0.20	0.10
	650.13	74.1	800	0.70	0.60
	625.14	71.1	860	0.70	0.54
	650.15	64.8	850	8.5	6.1
Halden	650.16	60	850	0.15	0
	650.3	81.9	850	medium & fine*	medium & fine*
	650.5	83	1100	medium & fine*	medium & fine*
	650.9	90	1100	medium & fine*	medium & fine*
	650.4	92	850	medium & fine*	medium & fine*
	HBR#1	71 (66.5)+	1000	31.59	23.60
ORNL	NA#1	74 (67.3)+	1200	27.4	12.3
	NA#2	84 (75.1)+	1000	25.2	13.4

⁺Rodlet average burnup (father rod burnup) [8,40,41,44]

^{*}Medium & fine assume 100% < 1 mm particle sizes



b)

Fig. 23. Summary of the mass fraction of fuel < 1mm (%) as a function of a) rodlet average burnup and b) terminal temperature for all integral and semi-integral LOCA tests.

LOCA tests to date have predominantly used IR heating lamps to perform the temperature transient, and Halden used a mix of nuclear and electrical heating. One data gap is related to the performance of the fuel under nuclear vs. electrical heating conditions. The Halden LOCA tests indicate significantly less fragmentation than the NRC and ORNL LOCA tests. Halden operated the rodlets at an average linear heat rate of ~8–9 kW/m before powering down the reactor to perform the LOCA transient. Under these conditions, the fuel would have a radial temperature profile slightly above the coolant temperature, whereas electrically heated LOCA tests heat the fuel uniformly to 300°C prior to the transient. Fuel operating in a PWR would be expected to operate at powers of ~15–25 kW/m, which would result in a

large portion of the pellet operating at temperatures above 800°C with a temperature gradient. During a LOCA, PCT results [19,20,47] suggest that the PCT throughout the core would range from 750–850°C. This would indicate that regions of the fuel would decrease in temperature, and other regions of the fuel may slightly or significantly increase in temperature. Future work should consider identifying the effects of pretransient and transient fuel rod conditions, if any, and focus on bridging the gap between nuclear and electrically heated LOCA tests.

Once fragmented, the fuel can potentially relocate into the balloon region and could possibly disperse through the burst opening. Halden LOCA tests were originally designed to evaluate the impact of fuel relocation into the balloon in order to assess the impact on PCT, so the LOCA experiments were designed to maximize ballooning [8]. The relocation and dispersal results for the Halden 650.X test are shown in Fig. 24. Fuel relocation appears to be a function of two parameters. The first is balloon or radial strain, and the second is burnup. Balloon strain results indicate fuel relocation requires a strain in excess of 40%. Secondly, fuel relocation was not observed in lower burnup rodlets of <72 GWd/tU. Once the burnup exceeded 72 GWd/tU, the fuel began to fragment into fine particles (i.e., <1 mm) that were small enough to relocate into the balloon region. Another observation shown in Fig. 24 is that fuel relocation occurred as a result of fuel falling from the upper regions of the rodlet. This is most noticeable in IFA 650.4 and 650.9, rods with burnups at or exceeding 90 GWd/tU, where large amounts of fine fragments were observed. These results suggest that a large balloon is required for gravity to actively relocate the fragmented fuel, and fuel fragments are required to be small enough for relocation to occur. This phenomenon was observed in the NRC-sponsored LOCA test [8]. PIE following the NRC-sponsored LOCA tests indicated that fuel in the upper regions of the rodlet severely fragmented and relocated into the balloon region.

DRAFT

Fig. 24. Summary of the Halden 650.X test series relocation and dispersal behavior [11].

Lastly, fuel dispersion was quantified during the NRC-sponsored LOCA test, see Table 3. Fuel dispersal was quantified in two categories: post LOCA bending and shacking. The second category does not represent the accident scenario and is considered overly conservative. Table 3 only considers fuel dispersal during the LOCA as it provides an accurate one-to-one comparison to a hypothetical PWR LOCA scenarios. Tests performed at Halden and ORNL reported fuel dispersal through activity detection and visible observations. NRC-sponsored LOCA test data indicate that fuel can disperse from the cladding during a LOCA transient, and it was determined that wet fuel was less prone to dispersal compared to dry fuel (i.e. fuel in the absence of steam or water). Once cladding failure occurs, fuel may be initially dispersed. However, subsequent relocated fuel will be exposed to water/steam which could act as a mobility inhibitor, thereby reducing the potential consequences. Sieving was not performed on the dispersed fragments, so it is not possible to determine the size of the fragments dispersed from the cladding. However, it may be possible to speculate about the size of the fragments dispersed from the cladding. Fig. 25 summarizes the area of the burst opening (defined as length times width) as a function of burst temperature and stress. Considering that a pellet has an approximate area (defined as fuel diameter times fuel height) of 80 mm², it would seem unreasonable to suggest that an intact or half fuel pellet could be dispersed from a burst opening <80–100 mm². Referencing the NRC LOCA test, it is clear that, irrespective of the fragment size, the area of the burst opening is such that ~2 intact pellets could fit through the burst opening. Of course, the fuel pellets in the burst region would need to fragment into smaller fragments for the reported amount of fuel to be dispersed. However, the burst opening is so large

that fuel, whether finely or coarsely fragmented, could be dispersed from the opening. As shown in Fig. 24, fuel dispersal was observed in IFA 650.4, 650.5, and 650.9. These tests reported that the fuel had extensive medium and fine fragments, along with a large balloon and burst opening of >275 mm². However, the amount of fuel dispersal was not quantified. The remaining IFA LOCA test reported some fuel dispersal, but it was reported that fuel dispersal was in the form of fine powder [11,54–62]; no medium or coarse fragments were reported to have dispersed. The one exception is in IFA 650.15, which had the largest reported burst opening. However, the activity measured outside the rod was similar to that reported for IFA 650.10. A potential reason for this might be the fraction of the coarsely fragmented fuel, ~91.5%. Lastly, ORNL used visual observations to evaluate fuel dispersal, and minimal dispersal was observed. There are two key conclusions from this data. Fuel dispersal requires the fuel to fragment into <1 mm particles for significant dispersal to occur, and cladding burst openings <80 mm² result in very little fuel dispersal, whereas large burst openings >100 mm² are required for extensive fuel dispersal, irrespective of fragment sizes.

Table 3. Fuel dispersal data summarized from the NRC-sponsored LOCA test

Rodlet	Burnup (GWd/tU)	Rupture dimensions (width/length) (mm)	Initial fuel mass (g)	Fuel mass loss during LOCA transient (g)	Fuel mass loss during LOCA transient (%)
189	72 (68.2)+	10.5 / 23.9	~150	41	27.3
191	75 (69.3)+	17.5 / 21.6	~150	52	34.6
192	78 (68.2)+	9 / 22.7	~150	68	45.3
193	76 (69.2)+	13.8 / 17.8	~150	105	70
196	61 (55.2)+	0.2 / 1.5	~150	0	0
198	60 (55.2)+	1.6 / 11	~150	0	0

^{*} Rodlet average burnup (father rod burnup)

Fig. 25. LOCA test burst length-to-width ratio as a function of burst temperature and burst stress [8,11,34,39,40,54–62]

3.4 Data Gaps and Open Questions

FFRD data generated through the various LOCA test programs have been used to identify a number of phenomena that impact FFRD and the resultant consequences. The key phenomena observed in high burnup LOCA testing are as follows:

- **Fuel rod bending:** Bending was observed in rodlets with a pre-transient rod internal pressure. The severity of bending increased with rod internal pressure.
- Cladding ballooning: The extent of cladding ballooning relies primarily on pretransient conditions (i.e., rod internal pressure) and heating rate. Increasing heating rates results in smaller balloons, and inversely, slower heating rates result in larger balloons. Cladding balloon data in integral and semi-integral LOCA tests to date are specific to heating rates of 5°C/sec or less.
- Cladding burst: The experimental data demonstrate a strong correlation between burst stress and burst temperature. Heating rates shift the correlation, with slower heating rates resulting in lower burst stresses than higher heating rates.
- Fuel rod depressurization: The rate at which the rodlets depressurize appears to be related to the severity of fragmentation and likely the balloon size. Studsvik data indicated that fuel rod depressurization occurs at a slower rate as fragmentation severity and relocation increases, while Halden data suggest otherwise. The cause for this decrease is unknown at this time, but it may be related to the release of fission gas during the fragmentation process.
- **High burnup fuel fragmentation or pulverization:** Fragmentation severity was observed to increase as the pellet/rodlet average burnup increased. Terminal temperature appears to contribute to fragmentation severity.
- Fuel relocation: Data generated during the Halden IFA 650.X test series demonstrate that relocation is a function of fragmentation severity. Finely fragmented particles of <1 mm readily relocated as compared to medium and coarse fragments, NRC-sponsored LOCA tests led to similar observations: balloon hoop strain needed to exceed ~5% before fuel relocation could occur.
- Fuel dispersal: Fuel dispersal was highly correlated to burst opening and fragmentation severity. Burst openings >100 mm² dispersed large amounts of fuel, whereas burst openings <80 mm² dispersed very little fuel. Fuel fragments dispersed from the cladding were considered fine pellet fragments at <1 mm, with the exception of when the burst >100 mm².

The phenomena identified are highly correlated and reliant on each other. For example, the size of the cladding balloon impacts the size of the burst opening, fragmentation severity, and fuel relocation, all of which directly impact the amount of fuel being dispersed from the cladding. Therefore, it is critical to holistically evaluate FFRD. A critical review of the data has led to identification of the following data gaps:

- Does the axial weight impact cladding behavior (i.e., balloon/hoop strain, burst opening) during a LOCA transient? Do other axial forces such as spacer grids and other structures impact the cladding response?
- What is the impact of prototypic PWR heating rates on the cladding behavior (i.e., balloon/hoop strain, burst opening)? As highlighted above, heating rates used in the LOCA testing programs may not be appropriate for PWR application. Studies suggest that prototypic PWR heating rates range from 24–34°C/sec and then decrease to ~2–5°C/sec [19,20,47].
- What is the impact of pretransient fuel operating conditions (i.e., initial fuel temperature), and
 how is fragmentation behavior impacted by the temperature evolution during the transient?
 LOCA tests to date have primarily used electrical heating to simulate LOCA transients; Halden
 used partial nuclear heating and observed improved fragmentation performance. Identifying the

- key differences between electrical heating and nuclear heating will support development of test matricies focusing on the appropriate testing conditions.
- What is the terminal temperature dependence on high burnup fuel fragmentation? Does a correlation between terminal temperature and pellet average burnup exist? Best estimate LOCA analysis suggest that the PCT for high burnup fuel will be much lower than 1000 C and when considering potential uncertainties those temperatures could increase near ~750–850°C, whereas current fragmentation data have a wide range of data points for a variety of burnups at temperatures >1,000°°C. Data generated through the Halden test program suggest that lower terminal temperatures (i.e., PCT) generate less pulverized material.
- Can fuel dispersal be quantified as a function of burst size? Data suggest that fuel dispersal is a function of the burst area. Burst areas <80 mm² suggest that fuel dispersal is small, whereas larger burst areas >100 mm² suggest extensive fuel dispersal irrespective of fragmentation size.
- What is the role of transient FGR during the LOCA? To data, there is little to no data suggesting FGR impacts the performance of high burnup fuel under LOCA conditions, however, significant FGR may impact the cladding behavior (i.e. burst timing, balloon/hoop strain, burst opening) and subsequent fragmentation behavior.
- Finally, what happens to the dispersed fuel once ejected from the burst opening.

4.0 High Burnup Fuel Fragmentation Separate Effects Testing

4.1 High Burnup Fuel Sample and Disk Heating Tests

In the early 2000s, researchers began evaluating burst release behavior of 85Kr in UO₂ fuel with a fully developed rim structure, or high burnup structure (HBS) [64,65,77,78]. Specific rim structure characteristics suggested the formation of sub-micron size grains may enhance FGR during steady-state operation, and due to fission gas stored in the rim region, large amounts of fission gas could be released during a transient or off-normal heating conditions [64–72]. Out-of-pile heating technique with an emphasis on applying hydrostatic pressures under controlled conditions were also conducted. The aim was to investigate the impact of an external hydrostatic pressure on FGR and swelling of fission gas bubbles as well as heating rates. Two types of high burnup UO₂ structures were evaluated. The first structure was extracted from fuel irradiated in a commercial PWR at an average temperature of ~500-800°C, while the second structure was generated by irradiating UO₂ disk at an average temperature ranging from 550–700°C. Samples had an average burnup ranging from 36 GWd/tU up to ~200 GWd/tU. The samples were subjected to heating rates ranging from 0.210-4,600°C/sec under a variety of hydrostatic pressure conditions ranging from atmospheric to 150 MPa [65]. The results indicate that regardless of the ramp rate, FGR occurs once the temperature exceeds 700°C for burnups >74 GWd/tU. The reported mechanism driving FGR was attributed to microcracking and interlinking of bubbles in the rim region. Furthermore, extensive microcracking in the fuel sample subsequently led to fuel samples fragmenting and pulverizing. Higher burnup samples heated in a step wise fashion. Fuel samples with burnups <74 GWd/tU experience FGR only at terminal temperatures (>1000°C) and microcracking was not observed in these samples.

Through the Nuclear Fuel Industry Research (NFIR) program, Noirot et al. [77] irradiated a fresh UO₂ fuel disk sandwiched between two molybdenum disks in the HBWR to control the temperature in order to investigate the impact of fission gas localization and release behavior in high burnup fuel. The fuel disk was irradiated at ~700°C for the majority of the irradiation time to a final burnup of 103 GWd/tU. Prior to the temperature transient, the fuel sample microstructure was observed and compared to PWR fuel. The disk had completely transformed into HBS, and despite being unstressed, the disk had a microstructure similar to that of commercial PWR fuel: specifically porosity, Xe wt% in the grains, and average molar volume in the bubbles. The only notable differences between the fuel disk and commercial PWR fuel were that the average grains and bubble sizes were larger in the fuel disk. The root cause for the difference was never identified, but it was suggested that higher local temperatures and fission rate during

irradiation may have caused or contributed to the difference. The fuel disk was ramped to 300°C and held for ~15 minutes, and then it was ramped at a rate of 0.2°C/sec to 1,200°C. The experimental results shown in Fig. 26 indicate that FGR occurred in two stages. The first release of fission gas occurred at ~880°C, and the second release occurred at ~1,180°C. Two FGR mechanisms were identified. The first mechanism was a result of fuel fragmenting/microcracking into ~100 micrometer fragments, and the second mechanism is associated with FG diffusion from FG bubbles within the individual fragments. Results from work by Noirot et al. [77] are interesting, as they suggest that HBS forming at higher operating temperatures form larger grains and fission gas bubbles than those typically observed in commercial fuel; this effect was also observed in MOX [127,147] However, the temperature transient indicated that FGR driven by microcracking, and thereby fuel fragmentation, occurred at higher temperatures of ~880°C than the previously observed temperatures >550°C. As noted below, the HBFF/pulverization threshold is well below this temperature, and the results suggest that increasing the irradiation temperature may increase the temperature threshold for fragmentation.

Fig. 26. Instantaneous FGR for the 103.5 GWd/tU [77].

Key observations are listed below [64,65]:

- 1. The onset of FGR occurred at ~1,250°C under 10 MPa hydrostatic pressure for fuel with a burnup of 90 GWd/tU and a fully developed rim structure. It was noted that FGR occurred at higher temperatures for lower burnups (i.e., 20–44 GWd/tU) under atmospheric conditions.
- 2. FGR under isothermal heating conditions depended on hydrostatic constraint and HBS. Furthermore, the experimental results indicated that FGR reduced under 150 MPa hydrostatic pressure as compared to 10 MPa.
- 3. FGR strongly depended on the extent of rim structure and heating conditions (i.e., heating rate and terminal temperature). Experimental results indicated that growth and interlinkage of intergranular bubbles in the rim structure controlled FGR above threshold temperatures. Burst FGR that occurred in high heating rates >90°C /sec as a result of microcracking in the rim region. Microcracking subsequently led to fuel fragmentation and pulverization. Burst release and fuel fragmentation occurred in high burnup fuels of 74 and 86 GWd/tU, with a fully developed rim structure once the temperature exceeded 700°C.
- 4. The temperature threshold for the onset of FGR increased as the irradiation temperature increased. Experimental results indicated fuel samples irradiated at ~700°C had a ~880°C temperature threshold for FGR, ~180°C greater than the irradiation temperature. Referencing back to the samples irradiated at lower temperatures (~500°C), the temperature threshold for FGR is ~150-200°C greater than the irradiation temperature. These results suggest microcracking

observed during the temperature transient correlates to the temperature increase above the irradiation temperature.

4.2 High Burnup Single Pellet Heating Tests

Similar to the fuel sample and disk heating test, researchers begin extending the research to the pellet level to understand FGR. The primary goal was to investigate mechanisms contributing to FGR from high burnup fuel under simulated LOCA conditions [73,74,75, 76]. The investigation used a single UO₂ fuel pellet complete with cladding. Fuel samples were irradiated in a commercial PWR for four, five, six, and seven annual cycles, and the respective burnup of each fuel pellet was 48.5 [73], 57.4 [74], 71.8 [73], 82-83 [75,76] GWd/tU. Each sample was preheated to 300°C in argon gas and held for a brief period of time. Subsequently, each sample was heated at a specified heating rate; heating rates ranged from 0.2 to 20°C/sec to a terminal temperature of 1,000°C or 1,200°C. In some cases, a 0.5 mm axial slit was inserted into the cladding to simulate the impact of ballooning and burst on FGR. Time dependent FGR measurements were taken as a function of temperature. A sample of these results can be seen in Fig. 27 [73]. The results indicated that a FGR mechanism is coupled to an increase in burnup. Furthermore, the high burnup FGR mechanism occurs once the fuel temperature exceeds ~600°C, see Fig. 27b. Posttest evaluations indicated that there had been extensive microcracking in the high burnup samples which resulted in the FGR. FGR was observed in lower burnup samples (i.e. <71 GWd/tU), however, FGR only occurred at terminal temperatures, see Fig. 27a. These results echo the fuel sample and disk heating test results.

Marcet et al. [75] and Noirot et al. [76] performed heating test on single pellet samples where an axial slit was machined into the cladding. Both experiments identified a double hump burst release occurring during the heat-up phase, similar to Fig. 27b [75]. The onset release of fission gas occurred at ~550°C and completed at ~775°C, whereas the final release occurred near the terminal temperature. FGR was attributed to microcracking in the temperature regime of ~550–775°C. The magnitude of FGR was noticeably different between fuel samples where the cladding axial slit was present and samples where the cladding was intact. The sample containing the cladding slit had more FGR as well as extensive fragmentation. Fuel samples without an axial slit intact did not experience severe fragmentation. Fuel loss for the intact cladding samples was reported to be very minor and only occurring at the ends of the sample [75,76]. The sample containing an axial cladding slit fragmented into a wide range of fragment sizes and was expelled from the cladding slit.



Fig. 27. Instantaneous FGR for the a) 48.8 GWd/tU and b) 71.8 GWd/tU [73].

The key observations made by Y. Pontillon et al. are detailed below [46,73,74,75,76]:

1. FGR under simulated LOCA type conditions was attributed to the rapid release of fission gas from grain boundaries for burnups < 71.8 GWd/tU.

- 2. FGR mechanisms were specific to the interconnecting of fission gas bubbles. This mechanism resulted in either the volumetric growth of bubbles or over pressurization and subsequent grain boundary fracture.
- 3. Higher burnup fuel samples (> 71.8 GWd/tU) had a higher fractional release of fission gas than lower burnup samples (< 57.4 GWd/tU).
- 4. Microcracking did not occur in lower burnup fuel samples (< 48.8 GWd/tU), and FGR occurred once the temperature exceeded 1,000°C. High burnup samples (>71.8 GWd/tU) had a heating rate dependence associated with FGR and observed microcracking.
- 5. There was minimal intragranular contribution to FGR during the temperature transient for grain sizes on the order of $10 \mu m$.
- 6. Severe fragmentation was observed in fuel samples containing an axial cladding slit, and the fragmentation originated from the axial slit location. Fuel sample with intact cladding did not experience sever fragmentation or extensive fuel loss. Some fuel lost was observed at the ends of the intact sample. Reference 74 and 76 observed FGR and fragmentation in UO₂ samples extracted from the center of the fuel pellet.

Similar heating test were performed at Studsvik to verify the existence of an HBFF threshold by characterizing the fragmentation process as a function of burnup [63]. The Halden and Studsvik LOCA tests indicated a strong burnup dependence associated with HBFF. Fuel samples harvested from the Studsvik LOCA test parent rods; rod pedigrees were reported (see Table 4). Similar to previous work [46,75,76], fuel samples were extracted from the parent rods, and each sample encapsulated a half pellet on either side of an intact pellet within the cladding. Each fuel sample was approximately 20 mm long. It was noted that some fuel samples contained an axial slit in the cladding to reduce the radial restraint on the fuel sample. The axial slit was designed to simulate cladding ballooning. Lastly, two different heating rates were used: 11°C/sec and 16°C/sec up to 500°C, and 2.5°C/sec and 16°C/sec beyond 500°C.

Table 4 Fuel samples pedigree [63]

		Rod average	Cycle power (kW/m)					
Rod	Plant	burnup (GWd/tU)	1	2	3	4		
1	A	55	22.0	23.5				
2	В	68	24.5	23.1	5.0	14.8		
3	С	64	25.3	10.6	17.1	5.8		
4	С	74	26.4	17.4	12.5	11.7		

Observations indicated that fuel burnups less than or equal to 68 GWd/tU would not be susceptible to HBFF, but cracking may occur if unrestrained. Fuel samples harvested from rod 2 (local burnup of 72 GWd/tU) were incrementally heated to determine a temperature threshold to pulverization. The temperature increments were 650°C, 750°C, 800°C, and 850°C. Fuel loss was not observed at 650°C. Minor fuel loss was reported at 750°C, but it was noted that fuel loss originated from the ends of the sample. Fuel heated to 850°C experienced more fuel loss compared to the fuel heated to the other temperatures; however, the amount of fuel lost was not quantified. These results indicate that HBFF not only has a burnup threshold but also has a temperature threshold.

4.3 Summary of the High Burnup Fuel Heating Tests

Table 5 summarizes data generated through the various separate effects heating tests. Separate effects tests were designed to evaluate FGR from high burnup fuel samples and the existence of fuel fragmentation burnup thresholds under temperature transient conditions. Fuel samples extracted from PWR fuel and the fuel disk indicated that there are two mechanisms driving FGR during temperature transients. The first is a lower temperature (550–850°C) mechanism occurring as a result of FG bubbles

over-pressurizing and forming a network of microcracks, and the second is a higher temperature (>1,000°C) mechanism based on FG diffusion to free surfaces. Furthermore, these tests indicate a burnup threshold exists between 60 and 74 GWd/tU that renders the fuel susceptible to pulverization. However, fuel samples typically had a fully transformed high burnup microstructure. These results indicate that 74 GWd/tU local burnup could form a network of microcracks, eventually leading to fuel fragmentation and pulverization. Lastly, the data showed that applying a hydrostatic pressure would reduce FGR, and if high enough, it could mitigate FGR and microcracking.

Table 5Summary of the fuel sample and fuel pellet heating tests

	Pellet burnup (GWd/ MTU)	Sample burnup (GWd/ MTU)	Onset of FGR (°C)	Termination of FGR (°C)	Termination temperature (°C)	Observations	References
Fuel disk and		36	N/A	N/A	>800	No microcracking	65
samples cut from	N/A	60	N/A	N/A	>800	No microcracking	65
PWR		74	700	800	>800	Microcracking	65
fuel		86	600	800	>800	Microcracking	65
		103.5	880	1,180	1,200	Microcracking	77
	92	200	627	726	2,700	Microcracking	78
	48.5		1,200	1,200	1,200	No HBFF	73
	57.4		1,200	1,200	1,200	No HBFF	74, 75
	71.8		600	1000	1,200	Bust FGR	73
	83		550	775	1,200	Complete fuel loss	75
	>74 (74)*		550	850	1,000	Severely fragmented	63
Single pellet	61	N/A			1,000	No fuel loss reported	63
pener	68				1,000	No fuel loss reported	63
	71				650	No fuel loss reported	63
	71				750	Fuel loss from ends	63
	71				850	Slightly more fuel loss	63

^{*}Average father rod burnup

Single pellet heating test results echoed the small-scale test results. FGR and posttest observations of fuel pellets with an average burnup of 68 GWd/tU or less gave no indication of HBFF. HBFF was observed in fuel pellets with an average burnup of 71 GWd/tU. Minor fragmentation was observed, specifically at the ends of the sample, at 750°C, and there was slightly more fragmentation observed at 850°C. The extent of fragmentation was not measured, and visible observations were used to evaluate fragmentation. A transition appears to occur once the pellet average burnup exceeds 72 GWd/tU. FGR measurements from fuel pellets above 72 GWd/tU indicated that the onset of FGR occurred at ~550–600°C and terminated at ~800–850°C, as generally observed in Table 5. Again, visible observations were noted, and the extent of fragmentation was not measured. Therefore, it is not possible to definitively differentiate the fragmentation behavior between fuel pellets with an average burnup of 71 GWd/tU and fuel pellets with an average burnup >72 GWd/tU. There are, however, two possibilities that could stem from the

experimental observations. First is a binary fragmentation in which no fragmentation phenomenon occurs at 72 GWd/tU, or a gradual increase in mass fraction of fragmentation from 72 to >74 GWd/tU. The second possibility seems more likely, as the increase in fragmentation could be correlated to the radial burnup profile across the pellet; this implies that small-scale separate effects tests of fuel disks and PWR fuel pellet samples do translate to the pellet. Intact cladding samples performed remarkably better than fuel samples containing an axial slit in the cladding. It should be noted that fuel loss typically originated in the vicinity of the axial slit, but this was visually observed and never quantified.

It is possible to gain some insights from the fragmentation process by evaluating onset and completion of FGR during temperature transients. High burnup experimental observations identified microcracking as the mechanism driving FGR, so the onset of HBFF can be directly correlated to the onset and completion of FGR under the temperature transient conditions. Experimental data shown in Table 5 indicate that the onset of FGR occurs once fuel temperatures and burnup (pellet average) exceed ~550–650°C and ~71 GWd/tU, respectively. Furthermore, the onset of the FGR temperature threshold is inversely proportional to burnup. FGR persists until fuel temperatures exceeds ~800–850°C, the only exception being the fuel sample with the highest burnup of ~200 GWd/tU. For this sample, experimental data indicated that FGR terminated at ~726°C. However, data do not indicate when fuel microcracking transitions to fuel fragmentation and pulverization, so it seems reasonable to suggest that pulverization should occur either at the onset of FGR or at temperatures less than or equal to the temperature at which the rate of FGR is highest: ~700°C.

There is one outlier sample in Table 5 which performed better than the other fuel samples. Noirot et al. [77] irradiated a fuel disk to 103.3 GWd/tU at ~700°C, ~300–400°C higher than the typical temperatures observed in the rim region. The sample's microstructure was similar to those typically observed in PWR fuel, except that the size of the grains and FG bubbles were slightly larger than those observed in commercial PWR fuel. The fuel sample exhibited improved performance under a temperature transient, and the onset of FGR did not occur until ~880°C. One possible theory is that equilibrium FG bubbles in the fuel sample formed at higher temperatures, and in order for the FG bubble over-pressurization to initiate microcracking, fuel temperatures needed to increase ~180°C above the irradiation temperature. Some credence to this theory is given by considering the fuel samples extracted from the rim region operated at ~350–390°C. Data from these samples indicated that the onset of FGR occurred at ~160–200°C higher than the operating temperature. This suggests that FG bubble over-pressurization is the mechanism during the temperature transient that is imposing sufficient stress to fracture UO₂ and pulverize the material. However, additional data are required to verify this theory.

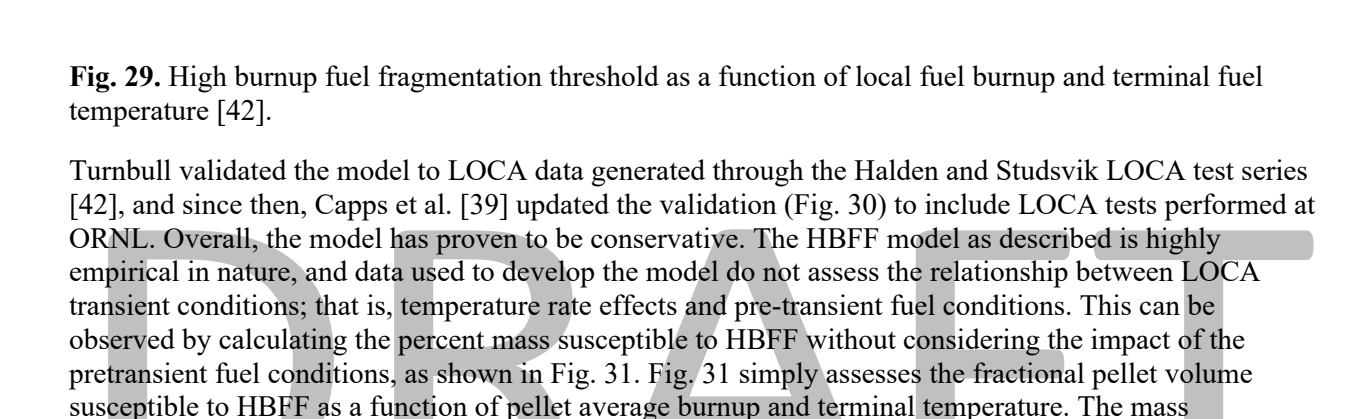
4.4 Fuel Sample Heating Test to Develop High Burnup Fuel Fragmentation Threshold

Through the NFIR program, Turnbull et al. set out to develop an HBFF threshold by building on the work discussed above [42]. The program proposed two sets of tests, and the culmination of these tests, along with the data described above, was used to develop an HBFF threshold. Like previous studies that analyzed hydrostatic pressure suppressing FGR, the primary purpose of the first test was designed to investigate the effect of hydrostatic pressures on fuel fragmentation and pulverization. Fuel samples were extracted from rodlets previously irradiated in the Halden reactor. Fuel samples were placed in a furnace similar to those used in the studies above. The samples were heated at a rate of 6,060°C/sec and 935°C/sec under specified hydrostatic pressures ranging from atmospheric to 150 MPa. A summary of the experimental results is shown in Fig. 28, and the Turnbull et al. results show increasing hydrostatic pressures suppresses FGR. PIE results indicated that fuel cracking and formation of small fragments decreased as the amount of FGR decreased. The complete experimental summary is reported by Turnbull [42].

Fig. 28. 71 GWd/tU FGR release as a function of hydrostatic constraint under extreme temperature ramp rate conditions [42].

The second objective was to develop a threshold for pulverization. This involved subjecting eleven fuel samples to laser heating. The fuel samples were extracted from fuel irradiated in a commercial PWR in which the pellet average burnup was equivalent to 76 and 93 GWd/tU. Fuel samples were cut from the center, mid-radius, and pellet periphery. The local burnups ranged from 62–66, 81–83, and >83 GWd/tU. Samples were mounted in a radio-frequency furnace and heated a rate of ~0.333–0.367°C/sec. Fuel sample temperatures were monitored with an optical pyrometer and heated until *fuel disruption* was observed. Turnbull et al. define *fuel disruption* as the sample moving from its original position and breaking into fragments and/or powder. Every fuel sample experienced some degree of fragmentation and pulverization, the extent of which depended on the sample burnup, as well as terminal temperature.

The pulverization threshold was developed by combining data generated through this study with data generated by Une et al. and Hiernaut et al. [64,65,78]. The combined data were used to develop the HBFF threshold shown in Fig. 29. The symbols on the figure represent the extent of pulverization, and they indicate the sources of the data. Samples in which pulverization occurred are denoted by solid squares, whereas solid triangles represent the onset of pulverization. *X* symbols indicate no pulverization. Symbol colors denote data taken from Une et al. and Hiernaut et al. [64,65,78], and black symbols are data generated through the NFIR program [42]. The line is the empirical threshold drawn to separate data that experienced disruption from data that did not experience disruption.



susceptibility is fairly mundane for low terminal temperatures: 636 and 800°C. Terminal temperatures

>917°C linearly increase the fractional pellet volume susceptible to HBFF to complete pellet pulverization from 74 to 78 GWd/tU. Therefore, these gaps in the model may result in overly conservative predictions of mass susceptibility to HBFF under prototypic PWR LOCA conditions.

Fig. 30. Summary of validation results for all publicly available integral LOCA tests performed on high-burnup fuel [39].

Fig. 31. Percent mass susceptible to HBFF as a function of pellet average burnup and terminal temperature.

4.5 Data Gaps and Open Questions

The HBFF data generated through the various separate effects programs helped to identify a burnup and temperature threshold. The data were harvested from local regions in PWR fuel, fuel disks irradiated in test reactors, and single pellets irradiated in commercial PWRs. Each sample was heated to a pretransient temperature of ~300°C and ramped under various temperature ramp conditions to a terminal temperature of ~1,000°C or higher. The data indicated the following:

- The onset of HBFF has been shown to initiate at local, nodal, burnups of 70–71 GWd/tU.
- Single pellet heating tests indicate that a pellet average burnup of ~72 GWd/tU is needed to induce HBFF on the pellet level.
- A temperature threshold is required to induce HBFF, and that temperature threshold decreases as a function of increasing burnup.
- The degree to which the extent of fragmentation occurs is dependent on the temperature ramp rate and terminal temperature.
- Hydrostatic pressures reduce FGR, and therefore HBFF. Given a high enough hydrostatic pressure—150 MPa—completely mitigates FGR, however, such high hydrostatic stress seems unrealistic.
- Single pellet samples that include an axial slit in the cladding exhibited HBFF, whereas samples without an axial slit in the cladding did not exhibit HBFF.
- Fuel disks were irradiated at high temperatures (~700°C), indicating that the temperature threshold for the onset of FGR increased from ~550–650°C to ~880°C.

However, applying the data and HBFF model to fuel operating in commercial PWR conditions highlighted the following data gaps:

- What is the impact of pretransient fuel conditions on pulverization, and do those conditions contribute to HBFF?
- Does fuel respond differently when local temperature differences between pretransient and peak transient differ by <150°C as compared to the same burnup with a delta temperature of >150°C?
- Does the pretransient temperature distribution and ensuing evolution during the LOCA generate additional stresses not captured by the Turnbull model? If so, does this stress contribute to HBFF?
- How does one quantify the hydrostatic pressure and/or cladding constraint applied by the rod internal pressure and/or cladding prior to ballooning and prior to burst?

• Are there operating conditions that generate microstructures that are more or less susceptible to HBFF?

5.0 High Burnup Fuel Microstructure Characteristics

5.1 Fuel Microstructure Features at High Burnup

Materials functionality is governed across the length scales by fabrication processing, chemistry, and microstructure. Nuclear fuels are no exception, but they come with an additional degree of complexity, as both chemical composition and microstructure vary in time as a consequence of damage accumulation and fission product transmutation, both during in-reactor operation and storage. Burnup and temperature gradients cause heterogeneous alteration and damage to the fuel matrix, such as grain growth, fission gas bubble precipitation, and extended defects formation. These processes act from the very beginning of irradiation, but they become increasingly important with exposure. The necessity to determine how fuel microstructure evolution impacts the engineering scale performance and safety limits is a long-standing problem that has driven efforts to incorporate such changes in fuel performance models and codes [79,80]. With the detection of HBFF, even more attention has been devoted to understanding the characteristics of the fuel's microstructure. Variation in features of the rim and the remainder of the pellet's microstructure are sought, as such variation could be the source of or could facilitate HBFF.

5.1.1 Microstructure at the Fuel Periphery: High Burnup Structure

High burnup microstructure is associated with the so-called rim or high burnup structure (HBS) formation, which is a microstructure transformation that starts to occur at the pellet's outermost radial periphery. This microstructure transformation in the pellet periphery is a consequence of enhanced ²³⁹Pu fission from neutronic self-shielding that increases local burnup (fission density) and boosts the accumulation of radiation damage. Although irradiation temperatures rise in the fuel during irradiation due to thermal conductivity degradation, the outer fuel temperature in a light water reactor stays below the limit for significant thermal recovery of irradiation damage [81]. As first observed in a few studies in the late 1950s-1960s [82-84], and as investigated again starting from the late 1980s [85,86], HBS is characterized by three main features: (a) the formation of submicrometric grains from the original grains [87,88], (b) the depletion of fission gas from the fuel matrix [89,90], and (c) a steep increase in the porosity [91–93], which retains most of the gas depleted from the fuel matrix in approximately spherical pores surrounded by rounded sub-grains[94–97]. An exponential relationship between pore density and burnup was discovered by Spino et al. [91] along the outermost part of the pellet radius, based on quantitative image analysis. The pore-diameter distribution at the rim peaks between 0.5–1 µm when the pellet average burnup is between 60 and 80 GWd/tU. The average size increases and the distribution broadens as burnup progresses. The pore number density increases, reaching a maximum at ~100 GWd/tU [98,99], at which time the number decreases. However, the bubble shape remains predominantly spherical, even at ultra-high burnup (i.e., local burnup >150 GWd/tU) [98–100]. Experimental reconstruction of fuel samples with local porosities of 24% showed no percolation of the HBS pore structure, confirming gas retention [101].

HBS gas behavior was a focal point, as the impact of FGR during off-normal conditions could impact integral fuel performance. An increase in porosity controls gas-driven swelling, worsening the cladding loading once pellet cladding contact occurs. Moreover, fission gas retention within the HBS could increase fuel centerline temperatures at high burnups through thermal conductivity degradation. Significant concern was expressed from industry, prompting further research to evaluate HBS formation conditions. In the early 2000s, it was determined that HBS formed once the fuel reaches a local burnup between 50–75 GWd/tU, whereas local temperatures remain below 1,100±100°C (Fig. 32) [97,102,103].

Fig. 32. Irradiation matrix of the High Burnup Rim Project (HBRP) highlighting the burnup and temperature thresholds for HBS formation [102].

The mechanism driving HBS formation has been long debated, particularly as it relates to the sequence between grain subdivision and micrometric bubble formation. Based on transmission electron microscopy (TEM) data for different fuels, Nogita et al. proposed grain-subdivision-aided Xe migration [104,105], whereas other authors proposed that grain subdivision starts at the surface of pre-existing, highly pressurized bubbles and then proceeds into the matrix [106]. This is supported by experimental evidence indicating that Xe depletion and bubble formation occur before grain subdivision [107]. The nature of the submicrometric grain has also been discussed. Matzke et al. [108], on the basis of observations of subgrains predominantly with low misorientation angle (e.g., < 15°), attributes HBS grain formation to a polygonization mechanism. Nogita et al. [105] refer to a recrystallization phenomenon instead, based on large grain misorientation in TEM studies. More recently, Gerczak et al. [109], employed electron backscattered diffraction (EBSD) to show that the majority of the grains has misorientation >15° in the fully recrystallized area. Adjacent to the fully transformed region, a low-misorientation—dominated area was observed instead, suggesting that low-angle grain boundaries would transition to high-angle grain boundaries once the microstructure fully transforms into HBS [109].

5.1.2 Evolution of the Microstructure outside the Rim

The vast majority of microstructural investigations have focused on the outermost part—the pellet periphery/rim region—of commercial fuel, where HBS formation starts. As burnup increases, the width of HBS progresses radially inwards. Various datasets collected on fuels with different designs and initial enrichment indicate that fully transformed HBS remains confined to $\approx 200 \,\mu m$ from the periphery, whereas the pellet average burnup remains below $80 \, \text{GWd/tU}^1$ [89,91,110–114]; HBS transformation rapidly increases, occupying up to 40% of the pellet's radius beyond $80 \, \text{GWd/tU}$ [115,116].

¹ Some discrepancies arise from the different techniques used to determine the HBS extension, depending on whether electron probe micro-analyzer (EPMA) signal depression or microscopy-based examination was performed.

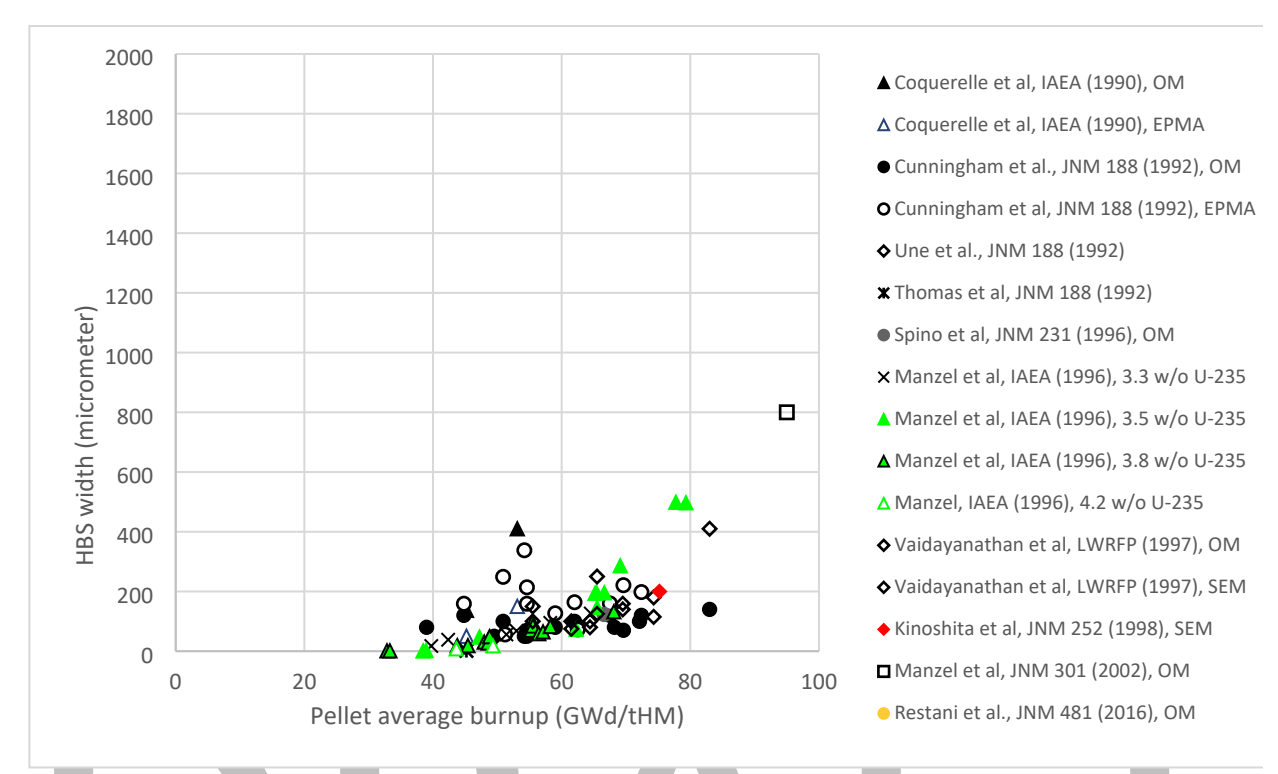


Fig. 33. Evolution of the HBS thickness vs. pellet average burnup.

Once the pellet average burnup exceeds 60–65 GWd/tU, the microstructural modifications are not restricted to the outermost fully transformed rim region, whereas transition zones and partial grain subdivision have been reported by several authors [94,107,109,111,114,117–120]. However, the pellet rim characteristics are consistent for all investigated fuels; modifications affecting the interior part of the pellet are less exhaustively and systematically documented in terms of grain structure and porosity quantification.

The extension of these secondary restructured or semi-restructured regions varies from study to study, depending on specimen burnup and specific irradiation conditions; in the majority of cases, these details are not available or are only partially publicly available. Most studies reported semi-transformed regions showing a mixture of original grains and subdivided grains preferentially located on initial grain boundaries [107,109,119] and open surfaces (e.g., surface of fabrication pores and fission gas bubbles) [109,119,121,122]. Polygonization has been observed across an entire fuel cross section irradiated for 9 cycles [120]. The nature and characteristics of such sub-grains (e.g., size and misorientation) is rarely reported, with the exception of two cases. Gerczak et al. [109] showed that at mid-radius and at the center of a specimen, with pellet average burnup 72 GWd/tU, low angle grain boundaries are dominating within the original grain networks. Noirot et al. [122] conducted EBSD analyses at the center of a specimen with 73 GWd/tU and showed that many subdomains with different crystal orientations had formed within the original grains.

Grain restructuring outside the rim is not the only phenomenon drawing attention to increased fragmentation at high burnup. Fission gas behavior plays a fundamental role, as well. Rapid over pressurization of bubbles causes the sudden rupture of grain boundaries and leads to HBFF. An extensive review of fission gas behavior in UO₂ fuel has been recently published [79], but it is outside the scope of this section. Here, the focus is on factors that play a major role and are crucial for validation of grain

boundary rupture criteria associated with HBFF, such as bubble size and size-distribution, shape, and initial fission gas content [123].

The exponential porosity increase due to HBS formation is a well-established characteristic of high burnup fuel and is considered a signature of HBS development. As for the grain structure evolution, porosity development at the center and at the intermediate radius is described mainly on a qualitative basis. Etching of fuel cross sections revealed the formation of various dark rings corresponding to an increased number of precipitated bubbles. Both the number and position of the rings are dependent on the pellet burnup, as well as irradiation conditions [124].

Not only the porosity, but also the pore number, density, and shape vary across the pellet radius. Generally, the higher the local porosity, the higher the local number density at intermediate and central radial positions. However, extrapolation of number density is complicated by the irregular shape of pores in these zones, limiting the applicability of stereological approaches [98]. Experimental 3D reconstruction based on focused ion beam (FIB) techniques [100,122] has recently proved complex pore morphology at the center of the pellet, which does not match the lenticular shape expected on grain boundaries. Studies to date are limited and have only considered samples with average pellet burnups of 72 and 73 GWd/tU, respectively.

Finally, bubble initial gas content in the form of initial pore pressure has been the focus of several studies. TEM-based energy-dispersive spectroscopy (EDS) [125,126], electron probe micro-analyzer (EPMA) and secondary ion mass spectrometry (SIMS) [127–129], or laser ablation inductively coupled plasma mass spectrometry (LA-ICP-MS) [116], all combined with image analysis, have been used to estimate bubble pressures starting from measured gas content and mean bubble size. A summary of the currently available data is shown in Fig. 34, where pressure is calculated from the reported atomic densities using Ronchi's equation of state (EOS) [130] at 300K. In addition to the datasets, equilibrium and dislocation punching pressures [126] are also shown. The datasets regard different types of bubbles: two studies focused on nanometric intragranular bubbles [125,126], and others focused on HBS bubbles [91,116,127,128] or on bubbles in the central zone of a 38.8 GWd/tHM Cr-doped fuel previously subjected to ramp testing [129].

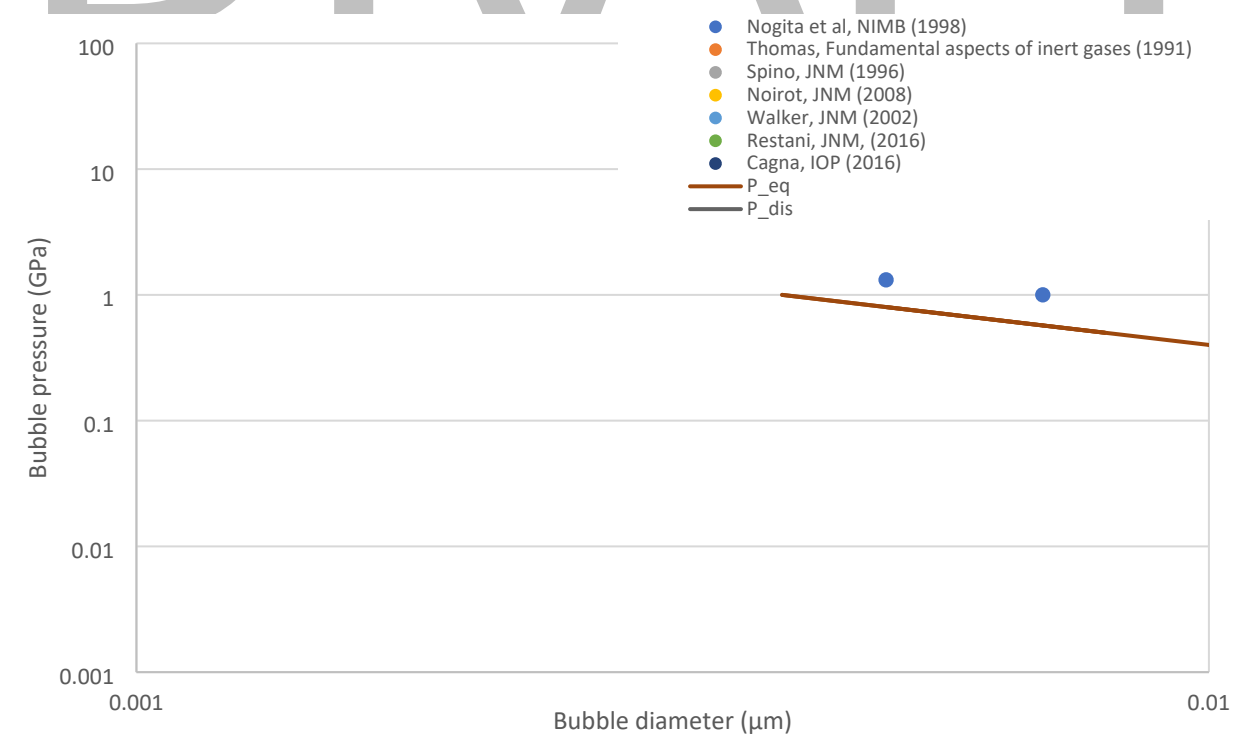


Fig. 34. Bubble pressure calculated with Ronchi's EOS at 300K from bubble size and atomic density reported in various studies. In addition, the equilibrium pressure and the dislocation punching pressure are also reported.

5.2 Implications for HBFF: Data Gaps and Open Questions

A thorough understanding of HBFF driving mechanism has been thwarted by at least two major factors. The first factor is the lack of definitive experimental information for key material properties and associated variation with irradiation. The second factor is the limited available information linking pretransient irradiation conditions to microstructural formation and status.

Staicu [131] has extensively reviewed the current knowledge of thermal properties of irradiated UO₂. Although the study of UO₂ is extensive, thermal conductivity data for LWR fuel at high burnups (>60 MWd/MTU) is limited due to the inherent difficulties of working with highly irradiated nuclear fuel [132–136]. Existing studies have often focused on the implications of HBS on thermal conductivity. UO₂ thermal conductivity is dominated by phonon-phonon interactions at temperatures relevant to LWR conditions. It is degraded by radiation effects that inhibit phonon transport such as lattice defects caused by fission damage, porosity, and dissolved fission gas, and it is enhanced by anything that improves phonon transport, such as metallic precipitates. All these mechanisms are microstructural features that have distinct development pathways dependent on highly localized irradiation conditions, including temperature; these factors are inextricably linked. Understanding how these features develop and impact thermal conductivity can better define the mechanisms driving HBFF.

HBS provides a positive effect compared to trends describing degradation of UO₂ thermal diffusivity with increased burnup [132]. However, HBS thermal diffusivity still remains below that of fresh UO₂. The recovery of thermal diffusivity is driven by the HBS grain formation process, which returns the HBS crystals lattice closer to the fresh condition [137]. However, the recovery of the lattice thermal transport might be offset by the exponential increase in porosity when the HBS forms. The evolution of thermal conductivity in HBS must be better understood, because improvement or degradation of thermal conductivity in the pellet periphery impacts fuel temperatures and influences many of the microstructural features discussed in Section 5.1. A gap remains in understanding of the other UO₂ layers that develop in high burnup fuel, such as the so-called *dark zone* and the *white zone*. The dark zone is thought to contribute heavily to fine fragments in HBFF, along with the rim [138]. Understanding thermal conductivity in these regions will provide insights to understanding mechanisms driving HBFF.

Some of the primary factors determining the susceptibility of the fuel to fragmentation are governed by the material mechanical properties, specifically fracture stress (or strength), fracture toughness and Young's modulus, which is used to calculate stress intensity factors that defines driver for crack initiation. The evolution of matrix mechanical properties of the fuel with burnup >50 GWd/tU is one area with numerous data gaps; the greatest impact on HBFF is related to the local fracture resistance of the matrix, in addition to the pressure exerted by the bubble. The microstructural complexities of irradiated fuel prevent from establishing a clear relationship between the macroscopic bulk mechanical properties and the local mechanical response at micrometric level. Hence, conventional bulk mechanical testing is ineffective in tackling the needed information, i.e., the local mechanical properties such as grain boundary fracture toughness, which can be substantially different from the bulk polycrystalline fracture toughness.

Only a handful of studies have been performed on irradiated UO₂ [139–142], mixed oxide (MOX) fuel [143], and doped UO₂ [Error! Reference source not found.]. A combination of acoustic microscopy [11,141Error! Reference source not found.] and microhardness [139], as well as dynamic nanoindentation [142] have been used to determine a general trend indicating that Young's modulus decreases as burnup increases. The increased porosity associated with high burnup is certainly a factor contributing to the Young's modulus trend since the presence of pores reduces the load-bearing area. However, a reduction solely driven by defect and fission product accumulation has also been shown, providing an empirical correlation with burnup and porosity [139,141]. Much less is known about the

local fracture stress and toughness of the matrix. Initial studies designed to investigate fracture toughness of high burnup UO₂ have been conducted by Spino and Matzke [140]. The results claim a toughening in the HBS rim zone, but fracture toughness is calculated from microindentation results, which is an unreliable methodology for this purpose [144]. More recently, Henry et al. [145,146] published the first fracture strength and toughness results based on micro-cantilever testing. The analyses of a Cr-doped UO₂ sample irradiated to 34 GWd/tU showed weaker grain boundaries on the periphery compared to interior grains, having a fracture strength 50% lower than the average measured within the grains at different crystallographic orientations. The non-doped sample, which was irradiated to 36 GWd/tU, exhibited a reduction of 85% in the grain boundary strength compared to the grain interior due to the presence of bubbles and precipitates on the grain boundaries. The material toughness seemed much less affected by the accumulation of fission product precipitates and irradiation defects [146]. All of these studies were performed at room temperature, so there is no knowledge of deformation mechanisms at reactor-relevant temperatures for irradiated UO₂. Overall, there is not enough experimental evidence to establish constitutive relationships that define the fuel mechanical response vs. irradiation damage and irradiation temperatures.

Qualitatively, it has been pointed out that the higher the amount of bubbles, the more prone the structure is to fine fragmentation [42,76], but the explanation is not exhaustive. Porosity, bubble size, shape, and fission gas content data are available, albeit sparse. However, there is no unambiguous correlation between pre-test power, microstructure formation, and fragmentation extent.

6.0 Summary

Integral LOCA experimental design and execution have identified significant differences between the high burnup LOCA tests performed at Halden, Studsvik, and ORNL. Halden used low power (~8 kW/m) nuclear energy to generate radial temperature profiles before transitioning to external electric heaters during simulated LOCA transients, whereas Studsvik and ORNL used IR lamps to externally heat rodlets. Heating rates for each test were restricted to 5 °C/sec and may not encompass the full spectrum of heating rates calculated in commercial PWRs, resulting in larger balloons than could be expected. Discrepancies or outliers were identified in the Studsvik LOCA tests as four rods bursting at premature temperatures and stresses, with all rods having larger balloon and burst sizes than compaired to historical data. The discrepancies may be correlated to the use of an axial weight being applied to the rodlet throughout the experiment in order to preserve the naturally straight nature of the rodlet; extensive data verify rodlets' propensity to bend as a result of cladding anisotropic creep and plasticity. Separate effects testing identified a pellet average burnup transition between 68 and 72 GWd/tU; HBFF begins to occur and become more prevalent above 72 GWd/tU. HBFF severity was also shown to increase with increasing terminal temperature, and the onset of HBFF occurred at ~550°C and terminated at ~850°C. Hydrostatic pressures and cladding restraint were shown to reduce and potentially mitigate HBFF. Microstructural analyses have strongly correlated the presences of HBS and high FG bubble density to HBFF. Notably, the correlations need additional data, particularly microstructural data connected to pretransient operating conditions.

A number of major data gaps were identified. The first is related to understanding fuel rod conditions (power, pressure, temperatures, etc.) prior to a LOCA transient. High burnup commercial fuel rods are expected to be irradiated for a period of four to six years, and throughout the irradiation period, the fuel in particular is subjected to temperature gradients, extensive irradiation damage, FG bubbles nucleation and growth, and grain subdivision. Fuel rod conditions as a whole are important, as well. All of these changes impact fuel performance throughout the LOCA and contribute to potential accident progression and subsequent consequences. Integral and separate effects tests under prototypic LOCA conditions were also identified as being needed. Integral experiments have not replicated the heating rates calculated for 4-loop Westinghouse PWRs, and while conservative, they may not adequately represent reality. Results from modeling and simulation analyses indicate that heating rates may range from ~25–35°C/sec down to ~8–10°C/sec, whereas integral LOCA heating rates to date range from <1–5°C/sec. Additionally, LOCA

analyses indicate that terminal PCTs are significantly less than 1,000–1,200°C, whereas integral LOCA tests have primarily focused on terminal temperatures >1,000°C. Halden has performed a few integral LOCA tests with representative terminal temperatures and has noted significant improvements. Determining the difference between nuclear and electrically heated integral LOCA tests was also identified as necessary. LOCA tests have never been initiated on high burnup rodlets operating at PWR LHRs with the appropriate LOCA thermal hydraulic boundary conditions, as these test conditions are difficult to replicate. Identifying synergies between nuclear and electrically heated LOCA tests as they relate to commercial PWR LOCA application would support accelerated testing, phenomenon identification, and resolution. Finally, holistic fuel rod performance has not been fully connected to fuel fragmentation, relocation, and dispersal severity. Conditions discussed above contribute to informing fuel rod performance (cladding ballooning, burst opening, potential relocation, fragmentation susceptibility, etc.). However, data to date fail to provide a comprehensive assessment—a coupled experimental and analytical assessment—to determine the dispersal severity and subsequent consequences.

7.0 Acknowledgments

This work was supported by the Advanced Fuels Campaign (AFC) of the US Department of Energy Office of Nuclear Energy. The authors would like to express their appreciation to Andrew Nelson and Christian Petrie for providing detailed technical feedback. Their feedback help improved the technical content of the manuscript.

8.0 References

- 1. Standard review plan for the review of safety analysis reports for nuclear power plants: LWR edition Transient and Accident Analysis (NUREG-0900, Chapter 15)
- 2. G. Rossiter M. Mignanelli, The characteristics of LWR fuel at high burnup and their relevance to AGR spent fuel, NNL (10) 10930 Issue 2, 2011
- 3. US Nuclear Regulatory Commission, Phenomenon identification and ranking tables (PIRTs) for loss-of-coolant accidents in pressurized and boiling water reactors containing high burnup fuel, NUREG/CR-6744, Washington, DC, December 2001
- 4. 895 FR 1184, Supplemental guidance regarding the chromium-coated zirconium alloy fuel cladding accident tolerant fuel concept February 10, 2020
- 5. US Nuclear Regulatory Commission, Cladding embrittlement during postulated loss-of-coolant accidents, NUREG/CR-6967, Washington, DC, July 2008
- 6. US Nuclear Regulatory Commission, Resolution of generic safety issues [formerly titled a prioritization of generic safety issues], NUREG-0933, Main Report with Supplements 1–33, Washington, DC, various dates.
- 7. *US Code of Federal Regulations*, Acceptance criteria for emergency core cooling systems for light-water nuclear power reactors, Title 10, Part 50, Section 46, January 1974 (amended)
- 8. P. A. C. Raynaud, (2012), Fuel fragmentation, relocation, and dispersal during the loss-of-coolant accident, NUREG-2121
- 9. US Nuclear Regulatory Commission, Acceptance criteria for emergency core cooling systems for light water nuclear power reactors, 10 CFR 50.46, Washington, DC, August 29, 2017
- US Nuclear Regulatory Commission, Accident source term, 10 CFR 50.67, Washington, DC, August 29, 2017
- 11. Report on fuel fragmentation, relocation, dispersal, Nuclear Energy Agency, Committee on the Safety of Nuclear Installations, NEA/CSNI/R(2016)16, October 2016
- 12. Nuclear fuel behavior in loss-of-coolant accident LOCA conditions: state-of-the-art report, OECD-NEA (2009), NEA No. 6846, ISBN 978-92-64-99091-3

- 13. F. Erbacher S. Leistikow, Zircaloy fuel cladding behavior in a loss-of-coolant accident: a review, in Zirconium in the Nuclear Industry, ed. R. Adamson, L. S. Van (West Conshohocken, PA: ASTM International, 1987), 451-488.
- 14. K.A. Terrani, D. Wang, L.J. Ott, R.O. Montgomery, The effect of fuel thermal conductivity on the behavior of LWR cores during loss-of-coolant accidents, J. Nucl. Mater. 448 (2014). doi:10.1016/j.jnucmat.2013.09.051.
- 15. C. Frepoli, K. Ohkawa, R. Kemper, , Realistic large break LOCA analysis of AP1000 with ASTRUM, The 6th International Conference on Nuclear Thermal Hydraulics, Operations, and Safety, Nara, Japan 2004, Paper ID N6P314
- 16. C. Frepoli, K. Ohkawa, K., et al., Realistic LOCA evaluation methodology applied to the full spectrum of break sizes (Full Spectrum LOCA Methodology), WCAP-16996-NP, Revision 0, November 2010. (ADAMS Accession Number ML103610227).
- 17. R. P. Martin, L. D. O'Dell, AREVA's realistic large break LOCA analysis methodology, Nuclear Engineering and Design 235 (2005) 1713–1725.
- 18. J. I. Sanchex, C. A. Lage, T. Nunez, LBLOCA analysis in a Westinghouse PWR 3-loop design using RELAP5/MOD3 U.S. NRC NUREG/IA-0195.
- 19. P. Raynaud, I. Porter, Predictions of fuel dispersal during a LOCA Proceedings of WRFPM 2014, Sendai, Japan, Paper No. 100026
- 20. H. Zhang, C. Blakely, J. Yu, R. Stewart, M. Asgari, Fuel rod burst potential evaluation under LOCA conditions for an existing plant with extended burnup exceeding the current limit by 20%, INL/EXT-19-55888, September 2019.
- 21. J. Montero-Mayorga, C. Queral, J. Rivas-Lewicky, J. Gonzalez-Cdelo, Effects of RCP trip when recovering HPSI during LOCA in a Westinghouse PWR, Nuclear Engineering and Design 280 (2014) 389–403.
- 22. N. Capps, R. Sweet, N. Brown, A. Wysocki, A. Godfrey, B. Collins, S. Lee, N. Szewczyk, S. Hoxie-Key, Full core LOCA safety for a PWR containing high burnup fuel, Nuclear Engineering & Design (2020), under review.
- 23. Aleshin, Y., Beard, C., Mangham, G., Mitchell, D., Malek, E., Young, M., 2010. The effect of pellet and local power variations on PCI margin, Proceedings of Top Fuel 2010, September 26-29, Orlando, FL, USA, Paper 041.
- 24. N. Capps, A. Mai, M. Kennard, W. Liu, PCI analysis of Zircaloy coated clad under LWR steady state and reactor startup operations using BISON fuel performance code, Nuclear Engineering and Design, Volume 332, 2018, 383–391.
- 25. N. Capps, S. Stimpson, K. Clarno, B. D. Wirth, J. Rashid, Assessment of the analysis capability for core-wide PWR pellet-clad interaction screening of Watts Bar Unit 1, Nuclear Engineering and Design, Volume 333, 2018, 131-14
- 26. N. Capps, M. Kennard, W. Liu, B. D. Wirth, J. Rashid, PCI analysis of a commercial PWR using BISON fuel performance code, Nuclear Engineering and Design, Volume 324, 2017, 131–142.
- 27. N. Capps, R. Montgomery, D. Sunderland, M. Pytel, B. D. Wirth, Evaluation of missing pellet surface geometry on cladding stress distribution and magnitude, Nuclear Engineering and Design, Volume 305, 2016, 51–63.
- 28. Z. Zhang, W. Jiang, J.E. Dolbow, et al. A modified moment-fitted integration scheme for X-FEM applications with history-dependent material data. Comput Mech 62, 233–252 (2018). https://doi.org/10.1007/s00466-018-1544-2
- 29. W. Jiang, B. W. Spencer, J. E. Dolbow, Ceramic nuclear fuel fracture modeling with the extended finite element method, Engineering Fracture Mechanics, Volume 223, 2020, 106713, ISSN 0013-7944.
- 30. Fuel Reliability Guidelines: Pellet-Cladding Interaction, EPRI Technical Report 1015453 (December 2008).

- 31. PCI analyses and startup ramp rate recommendations for Westinghouse fuel in Exelon PWRs, EPRI Technical Report 1012915 (April 2006).
- 32. M. Oguma, . Cracking and relocation behavior of nuclear-fuel pellets during rise to power. Nucl Eng Des 76 (1983) 35–45.
- 33. Halden LOCA test series trial runs IFA-650.1, Review July 2003.
- 34. C. Grandjean, A state-of-the-art review of past programs devoted to fuel behavior under LOCA conditions, part one, clad swelling and rupture assembly flow blockage, Technical Report SEMCA-2005-313. IRSN (2005).
- 35. W. Wiesenack, Summary of the Halden Reactor Project LOCA Test Series IFA-650, OECD Halden Reactor Project, HPR-380 (2013).
- 36. W. Wiesenack, Summary and comparison of LOCA tests with BWR fuel in the Halden Reactor Project Test Series IFA-650, OECD Halden Reactor Project, HPR-383 (2015).
- 37. M. Billone, Y. Yan, T. Burtseva and R. Daum, Cladding embrittlement during postulated loss-of-coolant accidents, NUREG/CR-6967, USNRC, Washington, DC, USA (2008).
- 38. M. Helin and J. Flygare, NRC LOCA tests at Studsvik. Design and construction of test train device and tests with unirradiated cladding material, Studsvik Report N-11/130, 2011, link https://www.nrc.gov/docs/ML1221/ML12215A431.pdf.
- 39. N. Capps et al. Integral LOCA fragmentation test on high-burnup fuel, Nuclear Engineering and Design (2020), under review.
- 40. M. Flanagan, P. Askeljung and A. Puranen, Post-test examination results from integral, high-burnup, fueled LOCA tests at Studsvik Nuclear Laboratory, NUREG-2160 (2013).
- 41. H. Sonnenburg, W. Wiesenack, et al. (2016). Report on fuel fragmentation, relocation, dispersal.
- 42. J. A. Turnbull, S. K. Yagnik, M. Hirai, D. M. Staicu and C. T. Walker, An assessment of the fuel pulverization threshold during LOCA-type temperature transients, Nuclear Science and Engineering, 179:4, 477-485, DOI: 10.13182/NSE14-20 (2015).
- 43. D. Jadernas, K. Yueh, M. Bales, D. Wachs, K. Terrani, K. Linton, N. Meacham, Sample selection report for the irradiation and post irradiation examination of ultra high burnup fuel, INL/EXT 17-44054 (2018).
- 44. S. J. Dagbjartsson, B. A. Murdock, D. E. Owen, P. E. Macdonald, Axial gas flow in irradiated PWR fuel rods, TREE-NUREG-1158, September 1977
- 45. Powers, D.A. and R.O. Meyer, Cladding swelling and rupture models for LOCA analysis, in NUREG-0630, 1980, U.S. NRC.
- 46. Chapman, R., 1978. Multirod burst test program: progress report. Oak Ridge, Tennessee; Springfield, Virginia, Dept. of Energy, Oak Ridge National Laboratory, US Nuclear Regulatory Commission.
- 47. F. J. Erbacher, H. J. Neitzel, H. Rosinger, H. Schmidt, K. Wiehr. Burst criterion of Zircaloy fuel claddings in a loss-of-coolant accident. In *Zirconium in the Nuclear Industry, Fifth Conference, ASTM STP 754, D.G. Franklin Ed.*, 271–283. American Society for Testing and Materials, 1982
- 48. E.H. Karb et al., KfK in-pile tests on LWR fuel rod behavior during the heatup phase of a LOCA, KfK-3028, October 1980. ISSN 0303-4003
- 49. E.H. Karb et al., LWR fuel rod behavior in the FR2 in-pile tests simulating the heatup phase of a LOCA, KfK-3346, March 1983. ISSN 0303-4003

- 50. M. Bruet et al., FLASH experiments in SILOE reactor: fuel rod behavior during LOCA tests, OECD-CSNI/NEA Experts meeting on water reactor fuel safety and fission product release in off-normal and accident conditions, Riso, Denmark, May 16–20, 1983
- 51. T.F. Cook, An evaluation of fuel rod behavior during Test LOC-11, NUREG/CR-0590, US Nuclear Regulatory Commission, Washington, DC, March 1979.
- 52. J.M. Broughton et al., PBF LOCA test series, test LOC-3 and LOC-5 fuel behavior report, NUREG/CR-2073, US Nuclear Regulatory Commission, Washington, DC, June 1981.
- 53. J.M. Broughton et al., PBF LOCA test LOC-6 fuel behavior report, NUREG/CR-3184, U.S. Nuclear Regulatory Commission, Washington, DC, April 1983
- 54. B. C. Oberlander, H. K. Jenssen and M. Espeland, PIE results from the high burnup (83MWd/kg) PWR segment after LOCA testing in IFA 650-5, Loen, Norway, 2008.
- 55. B. C. Oberlander and H. K. Jenssen, LOCA IFA650.9: PIE of the 90 MWd/kg PWR rod subjected to a high temperature transient, in Enlarged Halden Program Group Meeting, Storefjell, Norway, 2010.
- 56. B. C. Oberlander, H. K. Jenssen and N. O. Solum, LOCA IFA650.12: PIE of a BWR rod subjected to LOCA testing in the HBWR, in Halden Program Group Meeting, Halden, Norway, 2012.
- 57. B. C. Oberländer, H. K. Jenssen, PIE the rod from LOCA test IFA-650.13 on high burnup BWR fuel, HWR-1095, 2014.
- 58. B. C. Oberländer, H. K. Jenssen, PIE the rod from LOCA test IFA-650.14 on high burnup BWR fuel, HWR-1096, 2014.
- 59. B. C. Oberländer, H. K. Jenssen, PIE on a pre-irradiated PWR fuel segment LOCA-tested in IFA 650.15, HWR-1204, 2017.
- 60. B. C. Oberländer, H. K. Jenssen, Non-destructive post irradiation examination (PIE) of IFA-650.16, rod 16 after LOCA testing performed in the Halden Reactor, HWR-1241, 2019
- 61. H. M. Chung and T. F. Kassner, Argonne National Laboratory, Deformation characteristics of Zircaloy cladding in vacuum and steam under transient-heating conditions: summary report, USNC Report NUREG/CR-0344, July 1978.
- 62. J.C. Brachet, C. Toffolon-Masclet, C. Hamon, T. Guilbert, G. Trego, J. Jourdan, A. Stern, and C. Raepsaet. Oxygen, hydrogen and main alloying chemical elements partitioning upon alpha-beta phase transformation in zirconium alloys. Solid State Phenomena. (2011) 172–174. 753–759.
- 63. K.H. Yueh, N. Snis, D. Mitchell, and C. Munoz-Reja. Fuel fragmentation data review and separate effects testing, Proceedings of 2014 Water Reactor Fuel Performance Meeting, (WRFPM 2014), (2014) (784). Sandia, Japan.
- 64. K. Une, S. Kashibe, and A. Takagi. Fission gas release behavior from high burnup UO₂ fuels under rapid heating conditions, Journal of Nuclear Science and Technology, 43:9 (2006) 1161–1171, DOI: 10.1080/18811248.2006.9711208.
- 65. K. Une, S. Kashibe, and K. Hayashi. Fission gas release behavior in high burnup UO₂ fuels with developed rim structure, Journal of Nuclear Science and Technology, 39:sup3 (2002) 668–674, DOI: 10.1080/00223131.2002.10875557.
- 66. E. Thomas, C.E. Beyer, L.A. Charlot, J. Nucl. Mater., 188, 80 (1992).
- 67. Nogita, K. Une, J. Nucl. Mater., 226, 302 (1995).
- 68. M. E Cunningham, M. D. Freshley, D. D. Lanning, J. Nucl. Mater., 188, 19 (1992)
- 69. Une, K. Nogita, S. Kashibe, T. Toyonaga, M. Amaya, Proc. of the Int. Topical Mtg. on LWR Fuel Performance Portland, 1997, p.478.

- 70. C.T. Walker, J. Nucl. Mater., 275, 56 (1999).
- 71. M. Mogensen, J.H. Pearce, C.T. Walker, J. Nucl. Mater., 264, 99 (1999).
- 72. K. Une, M. Hirai, K. Nogita, T. Hosokawa, Y. Suzawa, S. Shimizu, Y. Etoh, J. Nucl. Mater., 278, 54 (2000).
- 73. Y. Pontillon et al., Experimental and theoretical investigation of fission gas release from UO₂ up to 70 GWd/tU under simulated LOCA type conditions, paper 1025, Proc 2004 Int. Meeting on LWER Fuel Performance, Orlando, Florida, September 19–22 (2004).
- 74. M. Marcet et al., Contribution of high burnup structure to fission gas release under transient conditions, paper 2005, Proc. Top Fuel, Paris, France, 6–10 September (2009).
- 75. M. Marcet, Etude de la fracturation mecanique de la structure a haut de combustion des combustible irradies (RIM) en traitment thermeque, Universite d'Aix-Marseille December 2010.
- 76. J. Noirot, Th Blay, J. Lamontagne, L Fayette, Y. Pontillon, et al.. Size and radial origin of fragments formed while heating a 83 GWd/t_U PWR fuel up to 1200 °C. HRP / WGFS LOCA Workshop, May 2015, Aix-en-Provence, France. cea-01599153.
- 77. J. Noirot et al., Fission gas release behaviour of a 103 GWd/t_{hm} fuel disc during a 1200°C Annealing Test, Journal of Nuclear Materials 446 (2014) 163–171.
- 78. J. Hiernaut, T. Wiss, J.Y. Colle, H. Thiele, C. Walker, .W. Goll, and J. Konings. Fission product release and microstructure changes during laboratory annealing of a very high burn-up fuel specimen. Journal of Nuclear Materials. 377 (2008) 313–324. 10.1016/j.jnucmat.2008.03.006.
- J. Rest, M.W.D. Cooper, J. Spino, J.A. Turnbull, P. Van Uffelen, C.T. Walker, Fission gas release from UO₂ nuclear fuel: A review, J. Nucl. Mater. 513 (2019) 310–345. doi:https://doi.org/10.1016/j.jnucmat.2018.08.019.
- 80. P. Van Uffelen, J. Hales, W. Li, G. Rossiter, R. Williamson, A review of fuel performance modelling, J. Nucl. Mater. 516 (2019) 373–412. doi:https://doi.org/10.1016/j.jnucmat.2018.12.037.
- 81. J.R. Lamarsh, No Title, in: Introd. to Nucl. React. Theory, Addison-Wesley Publishing Company, 1961: pp. 38–39.
- 82. J. Belle, Irradiation effects in uranium dioxide, in: J. Belle (Ed.), Uranium Dioxide Prop. Nucl. Appl., U.S. Government Printing Office (1961): 552–565.
- 83. M.L. Bleiberg, R.M. Bernman, B. Lustman, Effects of high burn-up on oxide ceramic fuels, in: Proc. Symp. Radiat. Damage Solids React. Mater., Venice, Italy (1962) 319–428.
- 84. W.K. Barney, B.D. Wemple, Metallography of UO2-containing fuel elements, 1958.
- 85. S.R. Pati, A. Garde, L.J. Clinka, Contribution of Pellet Rim Porosity to Low-Temperature Fission Gas Release at Extended Burnups, in: Top. Meet. LWR Fuel Perform., ANS (1988) 204–215.
- 86. B. Grapengiesser, A.R. Massih, O. Nylund, E. Patrakka, L. Hyden, S.O. Andersson, G. Ronnberg, High Burnup Fuel Evaluation Activities in Sweden and Finland, in: Top. Meet. LWR Fuel Perform., ANS (1988) 31–40.
- 87. I.L.F. Ray, H. Matzke, H.A. Thiele, M. Kinoshita, An electron microscopy study of the RIM structure of a UO₂ fuel with a high burnup of 7.9% FIMA, J. Nucl. Mater. 245 (1997) 115–123. doi:https://doi.org/10.1016/S0022-3115(97)00015-9.
- 88. K. Nogita, K. Une, High resolution TEM of high burnup UO₂ fuel, J. Nucl. Mater. 250 (1997) 244–249.
- 89. M. Coquerelle, C.T. Walker, UO₂ irradiated at extended burnup: fission gas release and correlated structural featres, in: Fuel Perform. High Burn. LWR React., International Atomic Energy Agency, Studsvik, Sweden (1990) 110–117.

- 90. K. Lassmann, C.T. Walker, J. van de Laar, F. Lindström, Modeling the high burnup UO₂ structure in LWR fuel, J. Nucl. Mater. 226 (1995) 1–8.
- 91. J. Spino, K. Vennix, M. Coquerelle, Detailed characterisation of the rim microstructure in PWR fuels in the burn-up range 40–67 GWd/tM, J. Nucl. Mater. 231 (1996) 179–190. doi:https://doi.org/10.1016/0022-3115(96)00374-1.
- 92. M. Ohisi, High burnup fuel behavior studies at NUPEC, in: I.A.E. AGENCY (Ed.), Fuel Perform. High Burn. LWR React., Stusdvik, Sweden (1990) 46–52.
- 93. D. Baron, Abnormal porosity buildup in the fuel periphery at high burn-up, in: HBEP Steer. Comm. Meet., Wengen, Switzerland (1986).
- 94. C.T. Walker, T. Kameyama, S. Kitajima, M. Kinoshita, Concerning the microstructure changes that occur at the surface of UO₂ pellets on irradiation to high burnup, J. Nucl. Mater. 188 (1992) 73–79.
- 95. C.T. Walker, Assessment of the radial extent and completion of recrystallisation in high burn-up UO₂ nuclear fuel by EPMA, J. Nucl. Mater. 275 (1999) 56–62. doi:https://doi.org/10.1016/S0022-3115(99)00108-7.
- 96. M. Mogensen, J.H. Pearce, C.T. Walker, Behaviour of fission gas in the rim region of high burn-up UO₂ fuel pellets with particular reference to results from an XRF investigation, J. Nucl. Mater. 264 (1999) 99–112. doi:https://doi.org/10.1016/S0022-3115(98)00474-7.
- M. Kinoshita, T. Sonoda, S. Kitajima, A. Sasahara, T. Kameyama, T. Matsumura, E. Kolstad, V. V Rondinella, C. Ronchi, J.-P. Hiernaut, T. Wiss, F. Kinnart, J. Ejton, D. Papaioannou, H. Matzke, High Burnup Rim Project: (III) Properties of rim-structured fuel, in: ANS (Ed.), Pro. In. Top. Meet. LWR Fuel Perform. (2004) 207–213.
- 98. F. Cappia, D. Pizzocri, A. Schubert, P. Van Uffelen, G. Paperini, D. Pellottiero, R. Macián-Juan, V.V. Rondinella, Critical assessment of the pore size distribution in the rim region of high burnup UO₂ fuels, J. Nucl. Mater. 480 (2016). doi:10.1016/j.jnucmat.2016.08.010.
- J. Spino, A.D. Stalios, H.S. Cruz, D. Baron, Stereological evolution of the rim structure in PWR-fuels at prolongated irradiation: dependencies with burn-up and temperature, J. Nucl. Mater. 354 (2006) 66–84.
- 100. C. McKinney, R. Seibert, G. Helmreich, A. Aitkaliyeva, K. Terrani, Three-dimensional bubble reconstruction in high burnup UO₂, J. Nucl. Mater. 532 (2020) 152053. doi:https://doi.org/10.1016/j.jnucmat.2020.152053.
- 101. J. Spino, D. Papaioannou, J.-P. Glatz, Comments on the threshold porosity for fission gas release in high burnup fuels, J. Nucl. Mater. 328 (2004) 67–70.
- 102. M. Kinoshita, T. Sonoda, S. Kitajima, A. Sasahara, E. Kolstad, H. Matzke, V. V Rondinella, A.D. Stalios, C.T. Walker, I.L.F. Ray, M. Sheindlin, D. Halton, C. Ronchi, HBRP II: Irradiation and examination to investigate rim-structured fuels, in: Int. Top. Meet. LWR Fuel Perform., Park City, Utah, 2000.
- 103. T. Sonoda, M. Kinoshita, I.L.F. Ray, T. Wiss, H. Thiele, D. Pellottiero, V. V Rondinella, H. Matzke, Transmission electron microscopy observation on irradiation-induced microstructural evolution in high burn-up UO2 disk fuel, Nucl. Instrum. Meth. B. 191 (2002) 622–628.
- 104. K. Nogita, K. Une, Radiation-induced microstructural change in high burnup UO₂ fuel pellets, Nucl. Instrum. Meth. B. 91 (1994) 301–306.
- 105. K. Nogita, K. Une, Irradiation-induced recrystallization in high burnup in UO₂ fuel, J. Nucl. Mater. 226 (1995) 302–310.
- 106. D. Baron, M. Kinoshita, P. Thevenin, R. Largenton, Discussion about the HBS transformation in high burn-up fuels, Nucl. Eng. Technol. 41 (2009) 199–214.
- 107. J. Spino, D. Baron, M. Coquerelle, A.D. Stalios, High burn-up rim structure: evidences that xenon-depletion, pore formation and grain subdivision start at different local burn-ups, J. Nucl. Mater. 256 (1998) 189–196.
- 108. H. Matzke, M. Kinoshita, Polygonization and high burnup structure in nuclear fuels, J. Nucl. Mater. 247 (1997) 108–115. doi:https://doi.org/10.1016/S0022-3115(97)00081-0.

- 109. T.J. Gerczak, C.M. Parish, P.D. Edmondson, C.A. Baldwin, K.A. Terrani, Restructuring in high burnup UO₂ studied using modern electron microscopy, J. Nucl. Mater. 509 (2018) 245–259. doi:https://doi.org/10.1016/j.jnucmat.2018.05.077.
- 110. S. Vaidyanathan, R.D. Reager, R.W. Warner, C. Martinez, Y. Shirai, Y. Iwano, High burnup fuel pellet performance, in: Light Water React. Fuel Perform., ANS, Portland, Oregon, 1997: pp. 471–477.
- 111. M. Kinoshita, T. Kameyama, S. Kitajima, H. Matzke, Temperature and fission rate effects on the rim structure formation in a UO₂ fuel with a burnup of 7.9% FIMA, J. Nucl. Mater. 252 (1998) 71–78.
- 112. M.E. Cunningham, M.D. Freshley, D.D. Lanning, Development and characteristics of the rim region in high burnup UO₂ fuel pellets, J. Nucl. Mater. 188 (1992) 19–27.
- 113. K. Une, K. Nogita, S. Kashibe, M. Imamura, Microstructural change and its influence on fission gas release in high burnup UO₂ fuel, J. Nucl. Mater. 188 (1992) 65–72. doi:https://doi.org/10.1016/0022-3115(92)90455-T.
- 114. L.E. Thomas, C.E. Beyer, L.A. Chariot, Microstructural analysis of LWR spent fuels at high burnup, J. Nucl. Mater. 188 (1992) 80–89. doi:https://doi.org/10.1016/0022-3115(92)90457-V.
- 115. R. Manzel, C.T. Walker, EPMA and SEM of fuel samples from PWR rods with an average burn-up of around 100 MWd/kgHM, J. Nucl. Mater. 301 (2002) 170–182. doi:https://doi.org/10.1016/S0022-3115(01)00753-X.
- 116. R. Restani, M. Horvath, W. Goll, J. Bertsch, D. Gavillet, A. Hermann, M. Martin, C.T. Walker, On the condition of UO₂ nuclear fuel irradiated in a PWR to a burn-up in excess of 110 MWd/kgHM, J. Nucl. Mater. 481 (2016) 88–100. doi:https://doi.org/10.1016/j.jnucmat.2016.08.023.
- 117. H. Matzke, J. Spino, Formation of the rim structure in high burnup fuel, J. Nucl. Mater. 248 (1997) 170–179.
- 118. S. Bengtsson, Examination of sub-grain formation in high burnup UO₂ fuel using the EBSP method, in: Adv. Fuel Pellet Technol. Improv. Perform. High Burn., 1996: pp. 177–183.
- 119. F. Cappia, Investigation of very high burnup UO₂ fuels in light water reactors, Technischen Universität München, 2017.
- 120. M. Chollet, G. Kuri, D. Grolimund, M. Martin, J. Bertsch, Synchrotron XRD Analysis of irradiated UO₂ fuel at various burn-up, in: TopFuel 2016, Boise, 2016.
- 121. N. Lozano, L. Desgranges, D. Aymes, J.C. Niepce, High magnification SEM observations for two types of granularity in a high burnup PWR fuel rim, J. Nucl. Mater. 257 (1998) 78–87. doi:https://doi.org/10.1016/S0022-3115(98)00056-7.
- 122. J. Noirot, I. Zacharie-Aubrun, T. Blay, Focused ion beam–scanning electron microscope examination of high burn-up UO₂ in the center of a pellet, Nucl. Eng. Technol. 50 (2018) 259–267. doi:https://doi.org/10.1016/j.net.2017.12.002.
- 123. L.O. Jernkvist, Modelling of fine fragmentation and fission gas release of UO₂ fuel in accident conditions, EPJ Nucl. Sci. Technol. 5 (2019). https://doi.org/10.1051/epjn/2019030.
- 124. R. Manzel, M. Coquerelle, Fission gas release and pellet structure at extended burnup, in: Light Water React. Fuel Perform., ANS, Portland, Oregon, 1997: pp. 463–470.
- 125. L.E. Thomas, Condensed-Phase Xenon and Krypton in UO₂ Spent Fuel, in: S.E. Donnelly, J.H. Evans (Eds.), Fundam. Asp. Nucl. React. Fuel Elem., 1991: pp. 431–442.
- 126. K. Nogita, K. Une, High resolution TEM observation and density estimation of Xe bubbles in high burnup UO₂ fuels, Nucl. Instruments Methods Phys. Res. Sect. B Beam Interact. with Mater. Atoms. 141 (1998) 481–486. doi:https://doi.org/10.1016/S0168-583X(98)00040-8.
- 127. J. Noirot, L. Desgranges, J. Lamontagne, Detailed characterisations of high burn-up structures in oxide fuels, J. Nucl. Mater. 372 (2008) 318–339. doi:https://doi.org/10.1016/j.jnucmat.2007.04.037.
- 128. C.T. Walker, S. Bremier, S. Portier, R. Hasnaoui, W. Goll, SIMS analysis of an UO₂ fuel irradiated at low temperature to 65MWd/kgHM, J. Nucl. Mater. 393 (2009) 212–223.

- doi:https://doi.org/10.1016/j.jnucmat.2009.06.017.
- 129. C. Cagna, I. Zacharie-Aubrun, P. Bienvenu, L. Barrallier, B. Michel, J. Noirot, A complementary approach to estimate the internal pressure of fission gas bubbles by SEM-SIMS-EPMA in irradiated nuclear fuels, IOP Conf. Ser. Mater. Sci. Eng. 109 (2016) 12002. doi:10.1088/1757-899x/109/1/012002.
- 130. C. Ronchi, Extrapolated equation of state for rare gases at high temperatures and densities, J. Nucl. Mater. 96 (1981) 314–328. doi:https://doi.org/10.1016/0022-3115(81)90575-4.
- 131. D. Staicu, 2.06 Thermal Properties of Irradiated UO₂ and MOX☆, in: R.J.M. Konings, R.E.B.T.-C.N.M. (Second E. Stoller (Eds.), Elsevier, Oxford, 2020: pp. 149–172. doi:https://doi.org/10.1016/B978-0-12-803581-8.11726-6.
- 132. C.T. Walker, D. Staicu, M. Sheindlin, D. Papaioannou, W. Goll, F. Sontheimer, On the thermal conductivity of UO₂ nuclear fuel at a high burn-up of around 100MWd/kgHM, J. Nucl. Mater. 350 (2006) 19–39. doi:https://doi.org/10.1016/j.jnucmat.2005.11.007.
- 133. C. Ronchi, M. Sheindlin, D. Staicu, M. Kinoshita, Effect of burn-up on the thermal conductivity of uranium dioxide up to 100.000 MWdt–1, J. Nucl. Mater. 327 (2004) 58–76. doi:https://doi.org/10.1016/j.jnucmat.2004.01.018.
- 134. J. Nakamura, M. Uchida, H. Uetsuka, T. Furuta, Thermal diffusivity of high burnup UO₂ pellet, International Atomic Energy Agency (IAEA), 1998. http://inis.iaea.org/search/search.aspx?orig q=RN:29059889.
- 135. M. Amaya, M. Hirai, H. Sakurai, K. Ito, M. Sasaki, T. Nomata, K. Kamimura, R. Iwasaki, Thermal conductivities of irradiated UO₂ and (U,Gd)O₂ pellets, J. Nucl. Mater. 300 (2002) 57–64. doi:https://doi.org/10.1016/S0022-3115(01)00704-8.
- 136. D. Staicu, V. V Rondinella, C.T. Walker, D. Papaioannou, R.J.M. Konings, C. Ronchi, M. Sheindlin, A. Sasahara, T. Sonoda, M. Kinoshita, Effect of burn-up on the thermal conductivity of uranium—gadolinium dioxide up to 100GWd/tHM, J. Nucl. Mater. 453 (2014) 259–268. doi:https://doi.org/10.1016/j.jnucmat.2014.07.006.
- 137. J. Spino, D. Papaioannou, Lattice parameter changes associated with the rim-structure formation in high burn-up UO₂ fuels by micro X-ray diffraction, J. Nucl. Mater. 281 (2000) 146–162. doi:https://doi.org/10.1016/S0022-3115(00)00236-1.
- 138. N.E. Agency, State-of-the-Art Report on Light Water Reactor Accident-Tolerant Fuels, 2018. doi:https://doi.org/https://doi.org/10.1787/9789264308343-en.
- 139. F. Cappia, D. Pizzocri, M. Marchetti, A. Schubert, P. Van Uffelen, L. Luzzi, D. Papaioannou, R. Macián-Juan, V. V Rondinella, Microhardness and Young's modulus of high burn-up UO₂ fuel, J. Nucl. Mater. 479 (2016) 447–454. doi:https://doi.org/10.1016/j.jnucmat.2016.07.015.
- 140. J. Spino, J. Cobos-Sabate, F. Rousseau, Room-temperature microindentation behaviour of LWR-fuels, part 1: fuel microhardness, J. Nucl. Mater. 322 (2003) 204–216. doi:https://doi.org/10.1016/S0022-3115(03)00328-3.
- 141. D. Laux, D. Baron, G. Despaux, A.I. Kellerbauer, M. Kinoshita, Determination of high burn-up nuclear fuel elastic properties with acoustic microscopy, J. Nucl. Mater. 420 (2012) 94–100. doi:https://doi.org/10.1016/j.jnucmat.2011.09.010.
- 142. K.A. Terrani, M. Balooch, J.R. Burns, Q.B. Smith, Young's modulus evaluation of high burnup structure in UO₂ with nanometer resolution, J. Nucl. Mater. 508 (2018) 33–39. doi:https://doi.org/10.1016/j.jnucmat.2018.04.004.
- 143. D. Laux, W. de Weerd, D. Papaioannou, S. Kitajima, V. V Rondinella, G. Despaux, Scanning acoustic microscope for mechanical characterization and density estimation of irradiated nuclear fuel, Prog. Nucl. Energy. 72 (2014) 63–66. doi:https://doi.org/10.1016/j.pnucene.2013.07.018.
- 144. G.D. Quinn, R.C. Bradt, On the Vickers indentation fracture toughness test, J. Am. Ceram. Soc. 90 (2007) 673–680. doi:10.1111/j.1551-2916.2006.01482.x.
- 145. R. Henry, I. Zacharie-Aubrun, T. Blay, S. Chalal, J.-M. Gatt, C. Langlois, S. Meille, Fracture properties of an irradiated PWR UO₂ fuel evaluated by micro-cantilever bending tests, J. Nucl.

- Mater. (2020) 152209. doi:https://doi.org/10.1016/j.jnucmat.2020.152209.
- 146. R. Henry, I. Zacharie-Aubrun, T. Blay, N. Tarisien, S. Chalal, X. Iltis, J.-M. Gatt, C. Langlois, S. Meille, Irradiation effects on the fracture properties of UO2 fuels studied by micromechanical testing, J. Nucl. Mater. 536 (2020) 152179. doi:https://doi.org/10.1016/j.jnucmat.2020.152179.
- 147. Y. Guérin, J. Noirot, D. Lespiaux, C. Struzik, P. Garcia, P. Blanpain, G. Chaigne, In Microstructure Evolution and in-reactor behaviour of MOX fuel, ANS International Topical Meeting on LWR Fuel Performance, Park City, Utah, USA; 2000
- 148. W. Li and K. Shirvan, "Multiphysics phase-field modeling of quasi-static cracking in urania ceramic nuclear fuel," Ceramics International, 2020, ISSN 0272-8842, https://doi.org/10.1016/j.ceramint.2020.08.191
- 149. C. M. Allision, G. A. Berna, R. Chambers, E. W. Coryell, K. L. Davis, D. L. Hagrman, D. T. Hagrman, N. L. Hampton, J. K. Hohorst, R. E. Mason, M. L. McComas, K. A. McNeil, R. L. Miller, C. S. Olsen, G. A. Reymann, and L. J. Siefken. SCDAP/RELAP5/MOD3.1 code manual, volume IV: MATPRO–A library of materials properties for light-water-reactor accident analysis. Technical Report NUREG/CR-6150, EGG-2720, Idaho National Engineering Laboratory, 1993.

DRAF!